Regulation by metal ions and the ADMIDAS of integrin α5β1 conformational states and intrinsic affinities

Running Title: **Metal ion regulation of integrin α5β1**

Jordan M. Anderson[1, 2], Jing Li[1, 2], and Timothy A. Springer[1, 2, *]

Affiliations

[1]Program in Cellular and Molecular Medicine, Boston Children's Hospital, Boston MA 02115

[2]Department of Biological Chemistry and Molecular Pharmacology, Harvard Medical School, Boston MA 02115

*Correspondence: Timothy A. Springer, springer@crystal.harvard.edu, ORCID 0000-0001-6627-2904, 3 Blackfan Circle, Center for Life Science 03-103, Boston MA 02115

Abstract

Activation of integrins by Mn^{2+} is a benchmark in the integrin field, but how it works and whether it reproduces physiologic activation is unknown. We show that Mn^{2+} and high Mg^{2+} concentrations compete with Ca^{2+} at the ADMIDAS and shift the conformational equilibrium toward the open state, but the shift is far from complete. Additionally, replacement of Mg^{2+} by Mn^{2+} at the MIDAS increases the intrinsic affinities of both the high affinity open and low affinity closed states of integrins, in agreement with stronger binding of Mn^{2+} than Mg^{2+} to oxygen atoms. Mutation of the ADMIDAS increases the affinity of closed states and decreases the affinity of the open state and thus reduces the difference in affinity between the open and closed states. An important biological function of the ADMIDAS may be to stabilize integrins in highly discrete states, so that when integrins support cell adhesion and migration, their high and low affinity correspond to discrete on- and off-states, respectively.

Highlight for TOC

Mn^{2+} activates integrins by increasing the ligand-binding affinity of all three of its conformational states by ~30-fold. Mn^{2+} also increases population of the high affinity state, but other states still predominate. The ADMIDAS increases the affinity difference between high and low affinity states and the fidelity of conformational change.

INTRODUCTION

Integrins are large, αβ heterodimeric membrane receptor glycoproteins that bind to the extracellular matrix (ECM) and surface of other cells and transmit signals and forces between the extracellular environment and intracellular cytoskeleton. Their α and β-subunits associate in a large, ligand-binding head and connect to transmembrane domains through multiple leg domains (Figure 1A). Most integrins, including α5β1, exist as ensembles with three distinct conformations: bent-closed (BC), extended-closed (EC) and extended-open (EO) (Springer and Dustin, 2012). Integrin affinity for extracellular ligands is tightly controlled by association with the cytoskeleton, which applies tensile force through ligand-bound integrins that stabilizes the high affinity, EO conformation (Li and Springer, 2017; Kechagia *et al.*, 2019; Sun *et al.*, 2019). The three integrin conformations interconvert by two distinct motions. (1) Change between the bent and extended conformations involves bending between the upper and lower legs in each subunit, i.e., between thigh and calf-1 in the α-subunit and between I-EGF1 and I-EGF2 in the β-subunit. (2) "Opening" of the ligand binding site, i.e., activation to its high affinity state, is achieved by conformational change within the β-subunit βI domain that is linked to a change in orientation at the βI domain-hybrid domain interface. The βI domain α1 and α7 helices each shift, with movement of the β6-α7 loop away from the active site and the β1-α1 loop toward the ligand-binding site (Figure 1A and B). These movements are linked to a change in orientation at the interface between the βI and hybrid domains (Takagi *et al.*, 2002; Xiao *et al.*, 2004; Luo *et al.*, 2007; Springer and Dustin, 2012; Su *et al.*, 2016; Dong *et al.*, 2017; Arimori *et al.*, 2021; Schumacher *et al.*, 2021).

The integrin βI domain has a unique arrangement of three closely-spaced metal ion binding sites, the metal-ion dependent adhesion site (MIDAS), the adjacent to MIDAS (ADMIDAS), and the synergistic metal ion binding site (SyMBS) (Figure 1B). In physiological conditions (~1 mM Mg^{2+}/~1 mM Ca^{2+}), the central MIDAS is occupied by Mg^{2+}, while the neighboring SyMBS and ADMIDAS bind Ca^{2+} ions (Xiong *et al.*, 2001; Xiao *et al.*, 2004). The MIDAS metal ion coordinates the Asp or Glu sidechain, the only invariant feature shared by all integrin ligands. The integrin α5β1 ligand fibronectin contains an Arg-Gly-Asp (RGD) motif that binds through its Asp sidechain to the MIDAS Mg^{2+} ion. The Mg^{2+} ion and Asp oxygen electron orbitals overlap, and thus their bond is partially covalent, particularly strong, and dominant over the Arg residue of RGD in regulating affinity (Xiao *et al.*, 2004; Zhu *et al.*, 2013; Lin *et al.*, 2016). The nearby Ca^{2+} ions in the ADMIDAS and SyMBS regulate ligand-binding affinity. Studies with multiple integrins have shown that low, ~50 μM concentrations of Ca^{2+} enhance binding and higher 1-10 mM concentrations of Ca^{2+} inhibit binding (Marlin and Springer, 1987; Staatz *et al.*, 1989; Dransfield *et al.*, 1992; Mould *et al.*, 1995a; Hu *et al.*, 1996; Labadia *et al.*, 1998; Chen *et al.*, 2003; Chen *et al.*, 2006; Valdramidou *et al.*, 2008). Mutational studies show that the SyMBS is the site at which low concentrations of Ca^{2+} enhance binding (Chen *et al.*, 2003; Chen *et al.*, 2006; Valdramidou *et al.*, 2008). Mn^{2+} has the remarkable ability to substantially enhance integrin binding (Gailit and Ruoslahti, 1988) and has been shown to replace Ca^{2+} and Mg^{2+} at the SyMBS, MIDAS, and ADMIDAS in crystal structures (Xiong *et al.*, 2002; Zhu *et al.*, 2013). Mn^{2+} competes with the inhibitory effect of Ca^{2+} and thus part of its effect may occur at the ADMIDAS (Chen *et al.*, 2003; Mould *et al.*, 2003a). α4β7 is an unusual integrin that mediates rolling adhesion as well as firm adhesion of leukocytes on vessel walls in vascular flow in Ca^{2+} and Mg^{2+}. In Ca^{2+}, α4β7 mediates rolling adhesion, whereas in Mg^{2+} and Mn^{2+}, it mediates firm adhesion. When ADMIDAS-coordinating residues are mutated, firm adhesion is abolished, but vigorous rolling adhesion is seen in Ca^{2+}, Mg^{2+}, and Mn^{2+} (Chen *et al.*, 2003).

Mould and Humphries have highlighted regulatory roles for the ADMIDAS and Mn^{2+} in integrin α5β1 (Mould *et al.*, 2002; Mould *et al.*, 2003a; Mould *et al.*, 2003b). Mutational removal of either one of the two Asp sidechains that coordinates the ADMIDAS metal ion reduced ligand binding affinity by 7 and 2.5-fold for Asp-137 and Asp-138, respectively and decreased the exposure of two epitopes in the hybrid domain that report headpiece opening, 15/7 and HUTS4, suggesting that the ADMIDAS was important in regulating or relaying conformational change between the βI and hybrid domains. Consistent with crystal structures (Xiong *et al.*, 2002), Mould and Humphries also inferred binding of Mn^{2+} at the MIDAS from effect of MIDAS mutations on binding of the 12G10 mAb to a nearby epitope that reports the open, high-affinity conformation of the βI domain.

Since the discovery of its enhancing properties (Gailit and Ruoslahti, 1988), Mn^{2+} has become a mainstay in integrin publications, particularly because of the relatively low affinity of integrins for ligands. However, how Mn^{2+} works is largely unknown. Mn^{2+} has been viewed on one hand as a positive control for a fully activated integrin, as fully opening integrins, and maintaining integrins in a high affinity conformation or on the other hand as shifting integrins toward the high affinity conformation.

Here, we address many important remaining questions about how Mn^{2+} and the ADMIDAS regulate integrin affinity using well-studied integrin α5β1 as our model. We have defined the nature of Mn^{2+}-induced integrin activation using recently developed methods that allow integrins to be stabilized in specific conformational states using conformation-specific antibody Fab fragments (Li *et al.*, 2017; Li and Springer, 2018) (Figure 1D and E). These methods allow the affinity of any ensemble of integrin states to be deconvolved into two components: 1) the intrinsic affinity of each integrin conformational state for the particular integrin ligand, and 2) the population in the ensemble of each conformational state (Figure 1D). Surprisingly, we find that Mn^{2+} both markedly increases the intrinsic affinity of the α5β1 EO state for ligand and also increases the population of the EO state within integrin ensembles on the cell surface and integrin ectodomain fragment ensembles in solution; however, the EO state is not completely populated. Thus Mn^{2+} shifts conformational ensembles but does not do so to completion. Our study also reveals an important contribution of the ADMIDAS to enhancing the large separation in affinity between the low affinity BC and EC states and the high affinity EO state and enhancing the fidelity of these states.

RESULTS

Influence of cations on intrinsic-ligand binding affinity and conformational equilibrium of soluble α5β1 ectodomain. Most experiments in this manuscript used highly purified wild-type or mutant α5β1 ectodomain fragments with high-mannose N-glycans (Figure 2A). Integrin stability was adversely affected by removal of metal ions and therefore we stored α5β1 at 20 to 100 μM concentrations (4 to 20 mg/mL) flash frozen in Tris-buffered saline (TBS) containing 1 mM $CaCl_2$ and 1 mM $MgCl_2$ and typically diluted it more than 1,000-fold in assays so that residual Mg^{2+} and Ca^{2+} concentrations were <1 μM (Methods); however, Ca^{2+} is present in laboratory de-ionized water at concentrations of ~5 to 10 μM. Fluorescence polarization (FP) of FITC-labeled fibronectin-mimetic peptides was used with integrin ectodomains to titrate metal ions (Figure 2B) or conformation-specific Fab fragments or measure ligand binding affinities. In FP assays, when a small fluorescent ligand binds to integrin, the FP signal increases because the integrin-ligand complex rotates more slowly than the free ligand and fluorescence emission retains a polarization closer to its excitation polarization. Thus, the FP value is directly related to the fraction of ligand that is bound to integrin. In an ensemble, FP is a function of (1) the intrinsic affinity of each conformational state for the ligand and (2) the population of each state in the ensemble (Figure 1D).

Accuracy of FP is dependent on the affinity of the ligand for the integrin or mutant in the particular metal ion conditions used and on binding sufficient ligand to have a good FP signal change while avoiding depleting free integrin at low integrin concentrations when integrin affinity is high. Therefore, we have used FITC-labeled, fibronectin-mimetic peptides that bind to α5β1 with lower affinity, GRGDSPK (RGD); or higher affinity, disulfide-cyclized ACRGDGWCG (cRGD) (Koivunen *et al.*, 1995).

Metal ion titrations with constant concentrations of ligand and α5β1 ectodomain revealed that Mn^{2+} and Mg^{2+} supported FITC-cRGD binding to α5β1 with EC_{50} values of 8 and 740 μM, respectively (Figure 2B). Above the EC_{50} values, the FP signal for Mn^{2+} was slightly higher than for Mg^{2+}, consistent with the higher ligand-binding affinity of α5β1 in Mn^{2+} than in Mg^{2+}, as shown below. In contrast, the FP value in Ca^{2+} remained low up to 100 mM, showing that Ca^{2+} is insufficient for ligand binding. However, we saw a slight increase in FP in Ca^{2+} titrations above ~50 μM, consistent with the small residual Mg^{2+} concentration from the purified integrin preparation and synergy between low concentrations of Ca^{2+}

and Mg^{2+} for supporting integrin ligand binding (Marlin and Springer, 1987; Mould *et al.*, 1995a; Labadia *et al.*, 1998; Chen *et al.*, 2003; Valdramidou *et al.*, 2008). In further experiments, we used 2 mM Mn^{2+} and 50 mM Mg^{2+}, which were ~100-fold above their EC_{50} values and thus sufficient to saturate the affinity-responsive metal-ion-binding site(s) of α5β1.

The concentration of a conformation-specific Fab required to saturably stabilize an integrin in a specific conformational state is directly related to the free energy of that state relative to the other states; higher energy states are less populated and require higher Fab concentrations to stabilize. Therefore, we determined EC_{50} values of Fab required to alter ligand binding affinity in 50 mM Mg^{2+} and 2 mM Mn^{2+} (Figure 3A-C and Table S1) to supplement values previously determined in 1 mM Mg^{2+}/1 mM Ca^{2+} (Li *et al.*, 2017). Based on these results, concentrations of conformation-specific Fabs at least 40 to 100-fold higher than their EC_{50} values were used in subsequent experiments to saturably stabilize specific conformation(s).

We next used FP to measure the affinities of different conformational states of the wild type α5β1 ectodomain for FITC-RGD in 50 mM Mg^{2+} and 2 mM Mn^{2+} and compared to previous measurements in 1 mM Mg^{2+} / 1 mM Ca^{2+} (Li *et al.*, 2017). In 50 mM Mg^{2+} and 2 mM Mn^{2+}, basal affinity for RGD was much higher than in 1 mM Mg^{2+}/Ca^{2+} (Figure 4A-C and Table 1). Furthermore, whereas Fabs that stabilized the extended and open states greatly increased the affinity of α5β1 ectodomain in 1 mM Mg^{2+} / 1 mM Ca^{2+} (Figure 4A), they increased affinity much less in 50 mM Mg^{2+} and 2 mM Mn^{2+} (Figure 4B,C). These results suggested that the EO state was much more populated in 50 mM Mg^{2+} and 2 mM Mn^{2+} than in 1 mM Mg^{2+} / 1 mM Ca^{2+}. The affinity of the closed states, BC+EC, was much lower, as shown with mAb13 (Figure 4A-C). To ensure that the concentration of mAb13 was high enough to saturably stabilize the closed states, two different mAb13 Fab concentrations were tested (Figure 4B-C). The very similar results confirmed that saturation was achieved. We were unable to express enough α5β1 ectodomain to use more than 10 µM concentrations (2 mg/ml) and therefore could not reach maximal ligand binding for all states in Figure 4. However, in each divalent cation condition, some integrin/Fab combinations gave maximal binding. By sharing the maximum value for all conditions in each panel in Figure 4, we achieved fit errors that were well below fit values (Table 1).

The calculated results of these measurements of the affinity of wild type α5β1 ectodomain for RGD in different metal ion conditions showed that Mn^{2+} did not completely stabilize the high affinity integrin state (Table 1, top left). The affinity for RGD of the basal ensemble (with all three conformational states) increased by 600-fold from 2300 nM in 1 mM Mg^{2+} / 1 mM Ca^{2+} to 3.9 nM in 2 mM Mn^{2+}. However, affinity was increased by two distinct mechanisms: an increase in the population of the EO state and an increase in its intrinsic affinity. The population of the EO state of the α5β1 ectodomain increased from 3.1% in 1 mM Mg^{2+} / 1 mM Ca^{2+} to 41% in 2 mM Mn^{2+}. Furthermore, the EO state intrinsic affinity increased from 71 nM in 1 mM Mg^{2+} / 1 mM Ca^{2+} to 1.6 nM in 2 mM Mn^{2+}. Although the results with 50 mM Mg^{2+} were largely intermediate between those with 1 mM Mg^{2+} / 1 mM Ca^{2+} and 2 mM Mn^{2+}, there was an interesting difference between the effects on population and intrinsic affinity. The population of the EO state was almost identical in 50 mM Mg^{2+} and 2 mM Mn^{2+}; however, the intrinsic affinity in 50 mM Mg^{2+} differed less from that in 1 mM Mg^{2+} / 1 mM Ca^{2+} (2.7-fold) than that in 2 mM Mn^{2+} (16-fold). Thus, while Mn^{2+} shifted only a portion of α5β1 ectodomain molecules to the EO state, the large increase in intrinsic affinity resulted in supraphysiologic activation. While shifting the entire integrin population in 1 mM Mg^{2+} / 1 mM Ca^{2+} to the EO state would result in an affinity of 71 nM, the basal integrin ectodomain ensemble in 2 mM Mn^{2+} has a substantially higher affinity of 3.9 nM.

Previous results on α5β1 ectodomain showed that its BC and EC states have identical ligand binding affinities (Li *et al.*, 2017; Li and Springer, 2018), and therefore we measured affinities for the combined BC and EC states here (Table 1, top left). The intrinsic affinity of the BC+EC states also increased in 50 mM Mg^{2+} and further increased in 2 mM Mn^{2+}. To buttress these results, and for direct comparisons to measurements on the ADMIDAS mutant, α5β1$^{D137A, D138A}$, later in this manuscript, we also measured affinities of wild type α5β1 for FITC-cyclic RGD, i.e., cRGD (Table 1, bottom left, Supplemental Figure S1). The results confirmed that 50 mM Mg^{2+} and 2 mM Mn^{2+} increased the

affinities for cRGD of the basal ensemble and the closed, BC+EC states (Figure S1). Affinities were well determined for low affinity measurements on the basal ensemble and on the BC+EC states and less well determined for the high affinity EO state, for which ligand depletion was significant and values have been omitted from Table 1. Mn^{2+} increased BC+EC affinity 150-fold compared to 1 mM Mg^{2+} / 1 mM Ca^{2+}. The BC+EC affinity of 1500 nM in 50 mM Mg^{2+} differed less from the affinity in 1 mM Mg^{2+} / 1 mM Ca^{2+} (4.7-fold) than from the affinity in 2 mM Mn^{2+} (33-fold) (Table 1), similar to the trend found for the EO state described in the previous paragraph.

Influence of cations on the conformational equilibrium of intact α5β1 on the cell surface. K562 cells express α5β1 as the only RGD-binding integrin. We were unable to measure fibronectin binding to cells, as we had done previously in 1 mM Mg^{2+} / 1 mM Ca^{2+} (Li *et al.*, 2017; Li and Springer, 2018), because its affinity for the EO state was too high to be accurately quantified in 2 mM Mn^{2+}. Furthermore, the fluorescence polarization experiments described above required four to six hours for RGD peptide to equilibrate with the EO conformation. Because cell viability declined during incubations in binding buffer on this timescale, we determined the conformational equilibrium of α5β1 on K562 cells by measuring the affinity of EO-specific Fab 12G10 for α5β1 ensembles on K562 cells as previously described (Li *et al.*, 2017). The affinity of these ensembles was proportional to their content (the population) of the EO state. As we were working with cells, which might release Ca^{2+}, we used 1 mM EGTA with the 50 mM Mg^{2+} condition.

We made two types of measurements. First, we measured binding of Alexa647-labelled 12G10 Fab after one hour at 21°C by flow cytometry without washing and subtracted background with the same concentration of Alexa647-12G10 Fab with a 500-fold excess of unlabeled 12G10 Fab. In these experiments, we measured Alexa647-12G10 Fab affinity for α5β1 on K562 cells in basal ensembles, the EC+EO ensemble in presence of 9EG7 Fab, and the EO state in presence of the fibronectin Fn3 domain 9-10 fragment (Figure 5A-C and 5G). However, we could not saturably populate the EO state in 1 mM Mg^{2+} / 1 mM Ca^{2+} without a large signal from unbound Alexa647-12G10 Fab. Therefore, in a second type of experiment we measured binding of a fixed concentration (10 nM) of Alexa488-labelled 9EG7 Fab as a reporter and were able to use 100-fold higher concentrations of Alexa647-12G10 Fab than in the first type of experiment to determine its affinity for α5β1 on K562 cells in basal ensembles in all three types of metal ion conditions (Figure 5D-F).

Although we measured affinity for 12G10 Fab in these assays and not affinity for fibronectin or RGD, several findings validate this method for measuring the population of conformational states and their free energies (Figure 5G). First, the different assays in Figure 5A-C compared to Figure 5D-F gave almost identical results for the basal ensemble affinities in 50 mM Mg^{2+} and 2 mM Mn^{2+}; their mean and difference from the mean are shown in Figure 5H. Second, the affinity of Alexa647-12G10 Fab for the EO state of α5β1 on K562 cells was almost identical (0.9 to 1.2 nM) and within error of the fit values in all three metal ions (Figure 5H). Third, the populations of the α5β1 BC, EC, and EO states on K562 cells in 1 mM Mg^{2+} / 1 mM Ca^{2+} of 98.8%, 1%, and 0.13%, respectively, was similar to that previously determined with binding to the fibronectin Fn3 domain 9-10 fragment of 99.8%, 0.05%, and 0.11% (Li *et al.*, 2017).

Overall, the results show that the population of the EO state in 1 mM Mg^{2+} / 1 mM Ca^{2+} of 0.13% increases to 1.8% in 50 mM Mg^{2+}/1 mM EGTA and to 4.9% in 2 mM Mn^{2+} (Figure 5H). The EC state also was more populated in 50 mM Mg^{2+} and in 2 mM Mn^{2+}. Similar to what was found with the ectodomain (Table 1), the EC state was more populated in 50 mM Mg^{2+} than in 2 mM Mn^{2+}(Figure 5H). On K562 cells, the energy of the BC state was increased relative to the EO state by ~2 kcal/mol in both 50 mM Mg^{2+}/1 mM EGTA and in 2 mM Mn^{2+} (Figure 5H), which was very similar to the effect observed with the same cations on the soluble ectodomain (Table 1). The cations also increased the energy of the EC state by ~1 kcal/mol (Figure 5H), which again was similar to the effect observed with the same cations on the soluble ectodomain (Table 1).

The ADMIDAS is important in activation of α5β1 by Mg^{2+} and Mn^{2+}. To test the role of the ADMIDAS metal ion in regulating ligand binding affinity and the integrin energy landscape, we mutated the only two residues with sidechains that coordinate the ADMIDAS metal ion in both the closed and open states, Asp137 and Asp138 (D8 and D9 in Figure 1B), to Ala (α5β1$^{D137A, D138A}$).

The ADMIDAS was essential for the inhibitory effect of Ca^{2+}. In the presence of a saturating concentration of 200 mM Mg^{2+} for WT α5β1, Ca^{2+} inhibited with an IC_{50} of 3.6 mM (Figure 6A). Calcium also reversed the activating effect of 2 mM Mn^{2+} and 50 mM Mg^{2+}, with IC_{50} values of 2.2 and 0.2 mM, respectively (Figure S3A). In contrast, Ca^{2+} had no inhibitory effect on α5β1$^{D137A, D138A}$ ectodomain, consistent with the ADMIDAS being the binding site responsible for the inhibitory effect of Ca^{2+} (Figure 6B). In agreement, the inhibitory effect of Ca^{2+} on α5β1^{WT} ectodomain was largely abolished by stabilizing its EO state with HUTS4 Fab, showing that Ca^{2+} inhibits by stabilizing closed states (Figure 6A). We further titrated Ca^{2+} in the presence of a physiological concentration of 1 mM Mg^{2+}. Again, Ca^{2+} was inhibitory for α5β1^{WT} but not α5β1$^{D137A, D138A}$ (Figure S4).

Influence of cations on intrinsic-ligand binding affinity and conformational equilibrium of soluble α5β1$^{D137A, D138A}$ ectodomain. Before attempting measurements on the conformational equilibrium of α5β1$^{D137A, D138A}$ ectodomain, we measured EC_{50} values for Fabs to determine concentrations required to saturably populate the open, closed, and extended conformations (Figure 3D-F). Results with mAb13 and 12G10, which stabilize the closed and open conformations of the βI domain by binding to the βI domain nearby the ligand binding site were as expected. However, SG/19 inhibits by binding distally from the ligand binding site to an interface between the βI and hybrid domains that is present in the closed but not open conformations (Nagae *et al.*, 2012). Most interestingly, in 1 mM Mg^{2+}/Ca^{2+} and 50 mM Mg^{2+}, SG/19 decreased FP with α5β1$^{D137A, D138A}$ ectodomain to a plateau level that was considerably higher than the plateau reached with mAb13 (Figure 3D,E), whereas mAb13 and SG/19 reduced FP to identical levels with α5β1 WT (Figure 3A,B). These results suggest that SG/19 stabilizes RGD-bound α5β1$^{D137A, D138A}$ ectodomain in two states, one with closed conformations of both the βI and hybrid domains, and the other with an open conformation of the βI domain at the ligand binding site and with other portions of the βI and hybrid domains in the closed conformation. The disconnect between these open and closed portions of the βI domain may occur near the mutated ADMIDAS. Curiously, in 2 mM Mn^{2+}, the SG/19 and mAb13 Fabs each decreased FP to similar levels (Figure 3F). However, while the effective concentrations of SG/19 and mAb13 Fab were similar in all other conditions (Figure 3A-E), in 2 mM Mn^{2+} the effective concentrations of SG/19 and mAb13 Fab were much higher and lower, respectively (Figure 3F).

The results with SG/19 Fab show that an intact ADMIDAS binding site is important for coupling between the βI domain and the hybrid domain. Similar results were seen with HUTS4 Fab, which also binds to a βI / hybrid domain interface but stabilizes the open conformation. HUTS4 was also less effective in activating the α5β1$^{D137A, D138A}$ ectodomain than the WT α5β1 ectodomain (Figure 4A-C compared to Figure 4D-F). Two Fabs, 8E3 and 9EG7, that bind to different knee-proximal leg domains to stabilize the extended conformations also had less clear effects with the α5β1$^{D137A, D138A}$ than the WT α5β1 ectodomain (Figure 3D-F).

Therefore, we measured affinities of α5β1$^{D137A, D138A}$ for RGD and cRGD in the three metal ion conditions only in the basal ensemble, the EO state, and the BC+EC states (Figure 4 and S5). EO affinities measured with cRGD with both mutant and WT α5β1 were nominally in the 0.1 to 2 nM range, where free integrin was significantly depleted which impeded accurate affinity measurement. Therefore, only RGD affinities for the EO state are reported in Table 1.

Compared to α5β1^{WT} ectodomain, the basal ensemble affinity of α5β1$^{D137A, D138A}$ ectodomain was lower for both RGD and cRGD (Table 1), consistent with the lower FP maxima reached by α5β1$^{D137A, D138A}$ than α5β1 WT in Mn^{2+} and Mg^{2+} ion titrations (Figure S3B). Interestingly, mutation of the ADMIDAS site changed metal-ion dependence for Mg^{2+} on affinity. Whereas 50 mM Mg^{2+} increased wild type α5β1 affinity 30 to 37-fold for the two ligands compared to 1 mM Mg^{2+}/ 1 mM Ca^{2+}, basal

ensemble α5β1$^{D137A, D138A}$ affinity was only increased 1.7-fold for RGD and showed indistinguishable affinities for cRGD (Table 1). 2 mM Mn^{2+} was still activating for α5β1$^{D137A, D138A}$ with both ligands, but to a lesser extent, with a 41- and 26-fold increase in affinity for the RGD and cRGD ligands, respectively, compared to 1 mM Mg^{2+}/ 1 mM Ca^{2+}.

Although we were unable to fully characterize the conformational ensemble of α5β1$^{D137A, D138A}$ ectodomain, we were able to make measurements on the high affinity EO state with RGD and the low affinity BC+EC states with cRGD (Table 1). Mn^{2+} increased the affinity of the α5β1$^{D137A, D138A}$ EO state for RGD by 12-fold and the affinity of the BC+EC states for cRGD by 55-fold compared to 1 mM Mg^{2+}/ 1 mM Ca^{2+}. Contrasting results were obtained with 50 mM Mg^{2+}. Compared to affinities in 1 mM Mg^{2+}/ 1 mM Ca^{2+} of α5β1$^{D137A, D138A}$, 50 mM Mg^{2+} decreased affinity of the EO state for RGD by 6-fold and the affinity of the BC+EC states for cRGD by 1.6-fold (Table 1). Most interestingly, the affinity for cRGD of α5β1$^{D137A, D138A}$ was higher than that of α5β1^{WT} in the BC+EC states, by 9-fold in 1 mM Mg^{2+}/ 1 mM Ca^{2+}, by 1.2-fold in 50 mM Mg^{2+}, and by 3-fold in 2 mM Mn^{2+}.

DISCUSSION

For decades, manganese has been extensively used in studies on integrins for its ability to activate them, without properly understanding its mechanism of action or how these Mn^{2+} activated integrins compare to physiologically activated integrins (Gailit and Ruoslahti, 1988; Ye *et al.*, 2012). In this paper, employing conformation-specific Fabs against the integrin β1 subunit to stabilize integrins into defined ensembles, we determined how cations influence the intrinsic ligand-binding affinity of each integrin conformational state and the equilibrium linkage between them. The conformational specificities of these Fabs were determined with negative stain EM (nsEM) with the integrin α5β1 ectodomain (Su *et al.*, 2016) and further verified by ligand binding affinity measurements in presence of saturating concentrations of Fab (Li *et al.*, 2017). In the latter study, we used between two to four independent antibodies or antibody combinations, often binding to distinct domains, to stabilize α5β1 ectodomain ensembles containing the EO, EC, EO+EC, and EC+BC states. In all cases, independent antibodies that stabilized the same conformational state(s) as determined by EM yielded similar ensemble *K*d values (Figure 3 in (Li & Springer, 2018; Li *et al.*, 2017), validating stabilization of the same state(s), and supporting the assumption that these states resembled those in the absence of Fab. Quantitatively, the antibodies must be highly state-specific in order to give large shifts in affinities, to give consistent intrinsic affinities on constructs with large differences in basal affinities, and to give similar intrinsic affinities using Fabs to distinct epitopes. The conformational specificity of these antibodies and their use at sufficient concentration to saturate these states are important for our previous thermodynamic studies {Li, 2017 #24745) and the current study.

We show that integrin α5β1 activation by Mn^{2+} or Mg^{2+} is caused both by an intrinsic increase in affinity of the active site and by a conformational shift of the integrin's ensemble towards the high affinity EO state. By mutating ADMIDAS-binding residues, we also show how the ADMIDAS influences intrinsic affinities of conformational states, integrin conformational equilibria, and links conformational change at the ligand binding site to swingout of the hybrid domain at its interface with the βI domain. Our results provide important insights into the functions of all three metal ion binding sites in the βI domain, which form the heart of the ligand binding site and govern its remarkable ability to change the affinity of α5β1 for ligands by 4,000-fold between the closed and open conformational states (Li *et al.*, 2017; Li and Springer, 2018).

Our results change the paradigm for how metal ions activate integrins. We found that in activating conditions with 2 mM Mn^{2+} or 50 mM Mg^{2+}, the conformational energy landscape was "flattened" compared to physiological concentrations of Ca^{2+} and Mg^{2+}, which are each near 1 mM, causing a shift in the population from the low affinity (BC and EC) states to the high affinity (EO) state. Contrary to a notion common in the literature, Mn^{2+} does not fully open integrins. Shifting the conformational equilibrium is one of the mechanisms, but it is not complete. Integrin α5β1 ectodomain preparations were 3.1% in the high affinity state (EO) in 1 mM Ca^{2+} / 1 mM Mg^{2+} (Li *et al.*, 2017; Li and

Springer, 2018) and were shifted in both 2 mM Mn^{2+} and 50 mM Mg^{2+} to 41% in the EO state. Intact α5β1 on cell surfaces is only 0.13% in the EO state and was shifted by 2 mM Mn^{2+} and 50 mM Mg^{2+} to 4.9% and 1.8% in the EO state, respectively. Intact α5β1 appears to be more stable than the ectodomain in the BC state because integrins in this state on cell surfaces associate extensively through their α and β-subunit TM and juxtamembrane domains (Lau *et al.*, 2009; Zhu *et al.*, 2009). Mn^{2+} and high Mg^{2+} increased the free energies of the BC and EC states of both intact and ectodomain forms of α5β1 by ~2 kCal/mol. The ectodomain was shifted more than the intact receptor on cell surface to the EO state because the free energy difference between the closed and EO states is lesser for the ectodomain. The similar effects on the BC and EC states suggest that 2 mM Mn^{2+} and 50 mM Mg^{2+} each exert their activating effect by favoring headpiece opening rather than integrin extension.

It is conceptually important to remember that the populations reported here are those in ensembles of unliganded integrins in the absence of ligand binding. Although our measurements use ligand, they measure the populations pre-existing before addition of ligand. Also, "population" is just a measure of the percentage of molecules in a particular state, and does not imply any difference between the molecules other than what conformation they are in. Indeed, it is essential to the validity of our thermodynamic formalism that all of the molecules are equally able to equilibrate from one state to another. Our results on populations of states in Table 1 are consistent with negative stain electron microscopy (EM) results that in the absence of bound ligand, integrin αVβ3 ectodomain particles were predominantly in the BC state in 1 mM Mg^{2+} / 1 mM Ca^{2+}, in both the EC and EO states in Mn^{2+}, and predominantly in the EO state in Mn^{2+} and cyclic RGD (Takagi *et al.*, 2002). The common use of Mn^{2+} to enhance ligand binding by integrins is explained by its ability to increase affinity of the α5β1 ectodomain for RGD and cRGD by ~400-fold. Recent cryo-EM structures of intact α5β1 in nanodiscs revealed the BC state in Ca^{2+} / Mg^{2+} in absence of ligand and the EO state in Mn^{2+} when bound to a fibronectin fragment (Schumacher *et al.*, 2021). While the authors were surprised to find that intact α5β1 was predominantly in the BC state in Mn^{2+} in absence of ligand, their finding is consistent with the observation here that intact α5β1 on the cell surface in Mn^{2+} is 93% in the BC state.

The increase in integrin intrinsic affinities for ligand in Mn^{2+} and Mg^{2+} was not previously anticipated and emphasizes the fundamental importance of the metal-oxygen bond between the MIDAS metal ion and the Glu or Asp in all integrin ligands in determining integrin affinity for ligand. Mn^{2+} and Mg^{2+} show octahedral coordination (six coordination positions) and distances of 2.2 Å from oxygens which promote partially covalent interactions. Mn^{2+} and Mg^{2+} both activate by binding to the ADMIDAS, and assuming that their effects are equivalent at that site, the difference in intrinsic affinities is attributable to the difference in energy of the MIDAS metal ion bond to the oxygen atom in the Asp sidechain of RGD. The energies of the Mn-O and Mg-O bonds will be influenced by their environments in solution and will be different yet at the MIDAS, where they are surrounded by a large network of hydrogen bonds. Nonetheless, a good approximation commonly used in chemistry to the difference in energies in solution is the difference in energy in the gas phase, which is 1.9 kcal/mol greater for Mn-O than Mg-O (Speight, 2016). The relationship between free energy (ΔG) and equilibrium constant (K_{eq}) shows an expected increase in affinity from replacing Mg^{2+} with Mn^{2+} at the MIDAS of 25-fold. The measured increases in intrinsic affinity in 2 mM Mn^{2+} compared to 50 mM Mg^{2+} of 16-fold for the EO state binding to RGD peptide and 33-fold for the EC+BC states binding to cRGD peptide compare well with the calculated value of 25-fold, supporting the hypothesis that the difference in energy between the Mn^{2+} and Mg^{2+} ligand bonds with oxygen is largely responsible for the higher intrinsic integrin affinity for ligand in Mn^{2+}.The increase in intrinsic affinity and shift in conformational equilibrium seen here in Mn^{2+} with α5β1 are expected to be similar in all other integrins, except for integrin αVβ8, which lacks an ADMIDAS.

Our results with α5β1$^{D137A, D138A}$ showed that alteration of the conformational equilibrium by Mn^{2+} and Mg^{2+} occurred primarily by their ability to displace Ca^{2+} at the ADMIDAS. Our finding that the α5β1$^{D137A, D138A}$ mutant lost its ability to be inhibited by Ca^{2+} agreed with previous results on integrins including α4β7, α2β1, α5β1, and αLβ2 (Chen *et al.*, 2003; Mould *et al.*, 2003a; Chen *et al.*, 2006; Valdramidou *et al.*, 2008). Previously α5β1^{D137A} and α5β1^{D138A} mutations were studied individually

(Mould *et al.*, 2003a); we mutated both of these residues in α5β1$^{D137A, D138A}$ to more completely remove metal ion binding.

We propose that differing coordination preferences of Mn^{2+} and Mg^{2+} compared to Ca^{2+} (Harding, 2001; Dokmanic *et al.*, 2008), which are matched to ADMIDAS coordination in open and closed integrin conformations, respectively, explain activation by Mn^{2+} and Mg^{2+}. Surveys of metal ion binding to proteins (Harding, 2001; Dokmanic *et al.*, 2008) show that as described above, Mn^{2+} and Mg^{2+} bind partially covalently to oxygen atom ligands at a typical distance of 2.2 Å, aligned octahedrally through electron orbitals (coordination number = 6). In contrast, Ca^{2+} binds to oxygen atoms electrostatically at a typical distance of 2.4 Å, with a preference for pentagonal bipyramidal (coordination number = 7) over octahedral (coordination number = 6). High resolution structures of integrin αIIbβ3 show that Ca^{2+} binds to the ADMIDAS with coordination number = 7 in the closed conformation, whereas in the open conformation, both Ca^{2+} and Mn^{2+} bind with coordination number = 6 (Springer *et al.*, 2008; Zhu *et al.*, 2012; Zhu *et al.*, 2013) (Figure 1C). ADMIDAS metal ion coordination to the backbone carbonyl group in the β6-α7 loop in the closed conformation is replaced by coordination to the sidechain carboxyl group of Asp-251 in the open conformation (Figure 1C). This change also favors the open conformation in Mn^{2+} and Mg^{2+}, since both metal ions strongly favor carboxyl over carbonyl oxygens, whereas Ca^{2+} coordinates well with both types of oxygens. These coordination preferences provide a mechanistic explanation for the ability of Mn^{2+} and Mg^{2+} to stabilize integrins in the open conformation.

Integrin αvβ8 lacks an ADMIDAS metal ion, and contains Asn residues in place of the ADMIDAS-coordinating Asp residues present in integrin β1 and the six other integrin β-subunits in mammals (Wang *et al.*, 2019; Campbell *et al.*, 2020). The βI domain β1-α1 loop and α1-helix contains the β-MIDAS motif, DXSXSXXDD (D1-S3-S5-D8-D9) (Wang *et al.*, 2019). Residues S5, D8, and D9 all coordinate the ADMIDAS metal ion and movement of this loop and the ADMIDAS metal ion toward the open state is hindered by ADMIDAS metal ion coordination to a backbone carbonyl oxygen in the βI domain β6-α7 loop (Fig 1B). When integrins are crystallized in absence of ligand and then ligand is soaked in, crystal lattice contacts inhibit hybrid domain swingout and frustrate βI domain opening, so that no movement, or partial opening to intermediate states, occurs (Zhu *et al.*, 2013). In crystals containing ADMIDAS-lacking integrin αvβ8, α1-helix movement is relatively large when ligand is soaked in. Furthermore, the affinity of the closed state of αvβ8 for ligand is higher than that of its sister integrin αvβ6, which has been attributed in part to lack of restraint by the ADMIDAS of α1-helix movement (Wang *et al.*, 2019). The finding here that the closed state of α5β1$^{D137A, D138A}$ has an affinity 9-fold higher than the closed state of α5β1^{WT} suggests that in the closed state of α5β1$^{D137A, D138A}$, the lack of ADMIDAS restraint allows its α1-helix to move further toward the MIDAS and thus reach higher affinity for ligand despite the overall closed state of the βI domain that was enforced by direct binding of the mAb13 Fab to the βI domain.

The quantitative studies here, together with recent affinity measurements and structure-function mutational exploration of integrin αVβ8, which uniquely among mammalian integrins lacks an ADMIDAS, provide insights beyond the well-known role of the ADMIDAS in transmitting conformational change and regulating ligand binding (Mould *et al.*, 2002; Chen *et al.*, 2003; Mould *et al.*, 2003a; Mould *et al.*, 2003b; Chen *et al.*, 2006). Our work suggests that the ADMIDAS is key for binary behavior of integrins in either being on or off, i.e., being in either high or low affinity states. Thus, we found that the low affinity, BC+EC state of the ADMIDAS mutant is 9-fold higher in affinity than that of WT, while its high affinity, EO state is 2.4-fold lower affinity than that of WT. Thus, while the high affinity state of WT α5β1 is 4,000-fold higher than its low affinity state, the high affinity state of the ADMIDAS mutant is only ~200-fold higher in affinity than its low affinity state. These results suggest that an important biological function of the ADMIDAS may be to provide a wide separation in affinity of integrin open and closed states. Our results with SG/19 and HUTS4 Fabs, which bind to interfaces between the βI and hybrid domains also demonstrate that an intact ADMIDAS is essential for maintaining the fidelity of conformational communication between the ligand binding site in the βI domain and its interface with the hybrid domain. Thus, in the context of binding of integrins on cells to substrates and providing

traction for supporting cell adhesion and cell migration, the ADMIDAS has an important role in ensuring fidelity in conformational communication within the integrin β-subunit and endows integrins with functional states that are akin to on and off states.

MATERIALS AND METHODS

Ligands. The ligands cyclic RGD peptide (ACRGDGWCG with N-terminal 6-aminohexanoic acid and cyclized by sidechain disulfide) and linear RGD peptide (GRGDSPK) were synthesized and labeled with FITC (fluorescein isothiocyanate) by GenScript. Stock solutions (10 μM) in DMSO were diluted with the appropriate buffer before use.

Integrin. Integrins used in these studies were expressed as the high-mannose glycan form using a stable HEK293S GnTI$^{-/-}$ (N-acetylglucosaminyltransferase I deficient) cell line (Li *et al.*, 2017). Both constructs (α5β1^{WT} and α5β1$^{D137A, D138A}$) contain α5 residues F1-Y954 and β1 residues Q1-D708. The ADMIDAS mutant was produced by replacement of a synthesized G-block (Integrated DNA Technologies) by 2-fragment Gibson assembly (HiFi, New England Biolabs) into the pD2529_CAG vector (ATUM). As previously described (Li *et al.*, 2017), α5 and β1 subunits were co-expressed with a C-terminal His-tagged leucine zipper, to aid expression and dimerization. Secreted proteins were purified from the clarified supernatant with a Ni-NTA column and eluted with high imidazole (300 mM). TEV cleavage removed the His-tag and leucine zipper and after a second run through a Ni-NTA column, the flow-through was concentrated and buffer exchanged with pH 7.4, 20 mM Tris, 150 mM NaCl (TBS) containing 1 mM $CaCl_2$ and 1 mM $MgCl_2$. Further purification was accomplished by size-exclusion chromatography (Superdex 200, GE Healthcare) in the same buffer, resulting in a single peak, which was concentrated to 20 to 100 μM, flash frozen, and stored at -80°C for future use. Typical final yield after purification for the mutant was 8 mg from 1 L culture supernatant. Integrins were not stored in the absence of metal ions, because gel filtration using running buffer containing EDTA or EGTA to remove divalent cations showed that a significant amount of the protein eluded in the void volume.

Fabs. Hybridomas were HUTS4 (Luque *et al.*, 1996), 12G10 (Mould *et al.*, 1995b), 8E3 (Mould *et al.*, 2005), 9EG7 (Lenter *et al.*, 1993), SG/19 (Miyake *et al.*, 1992) and mAb13 (Akiyama *et al.*, 1989). IgG produced from hybridoma was purified by protein G and digested with papain (500:1, IgG:papain) in pH 7, 20 mM sodium phosphate, 150 mM NaCl with 10 mM EDTA and 10 mM L-Cys at 37°C for 18 hrs. After buffer exchange with 50 mM Tris (pH 9), the Fab was purified by anion exchange chromatography (HiTrap Q HP, GE Healthcare), after which the fractions containing Fab were concentrated, flash frozen and stored at -80°C for future use.

FP assay. Fluorescence polarization measurements were made using a Synergy Neo plate reader (BioTek), with serial dilutions made in flat bottom black 384 well plates (Corning), with 10 μL samples. Samples were prepared in pH 7.4 buffer containing 20 mM Tris, 150 mM NaCl and the given concentration of Ca^{2+}, Mg^{2+}, Mn^{2+} or EGTA ($CaCl_2$, $MgCl_2$, $MnCl_2$ or ethylene glycol-bis(β-aminoethyl ether)-N,N,N',N'-tetraacetic acid), with 5 nM ligand and 20 nM integrin, unless otherwise noted. Since the stock solutions of integrin were prepared in 1 mM Ca^{2+} and 1 mM Mg^{2+}, for assays with different metal ions, samples were either diluted more than 1,000-fold into TBS with or without desired metal ions; alternatively, when used at less than 1,000-fold dilution, integrins were exchanged with the desired metal ion in TBS by diluting >10-fold with the desired buffer and concentrating 10-fold a total of 3 times. For metal ion titrations, the integrin was diluted in TBS and metal ion titrations were then added. To ensure that the binding was completely equilibrated, most readings were taken at 2, 4 and 6 hr, with negligible change found for the last two. When necessary, if excessively high concentrations of α5β1 were needed to saturate binding (e.g. α5β1^{WT} closed ensemble and α5β1^{D137A,D138A} basal ensemble), maximum values were shared with higher affinity conditions in the same experiment. A detailed explanation on the fitting of FP data and calculation of K_d or ΔG values can be found in Li et al. (Li *et al.*, 2017).

Cell surface binding assay. K562 cells (10^6 cells/mL in RPMI-1640 medium, 10% FBS) were washed twice with assay buffer (HBSS with 20 mM HEPES, pH 7.2, 1% BSA, and indicated cations) and suspended in assay medium. Each sample (50 µL) contained cells (2×10^6 cells/ml), Alexa647-12G10 Fab, and unlabeled 9EG7 Fab, or $Fn_3$9–10, or Alex488-9EG7 Fab in assay medium. The mixture was allowed to equilibrate for 1hr before flow cytometry (BD FACSCanto II) without washing. Direct measurement of Alexa647-12G10 Fab binding was recorded as mean fluorescence intensity (MFI) of Alexa647; background MFI was subtracted and was measured under the same conditions except with 500-fold higher concentration of unlabeled 12G10 Fab. Background subtracted MFI at different concentrations of AF647-12G10 in each metal ion condition was fitted to a dosage response curve to yield the K_d value of intact α5β1 for AF647-12G10. For the basal condition, affinity of Alexa647-12G10 Fab was also determined from enhancement of 10 nM Alexa488-Fn39–10 binding and fitted to dose response curve.

Supplemental Material. Supplemental material includes (5) Supplemental Figures and (1) Supplemental Table.

Acknowledgements.

Author contributions:

Conceived and Designed Experiments: JMA, JL, TAS
Performed the experiments: JMA, JL
Analyzed the Data: JMA, JL, TAS
Drafted the Article: JMA, JL, TAS
Prepared the Digital Images: JMA, JL, TAS

Funding: National Institutes of Health 1R01HL131729: *"Activation Trajectories of integrin α5β1"* (TAS and JL)

Data and materials availability. All data are available in the main text or the supplementary materials.

Conflict of Interest. The authors have declared that no conflict of interest exists.

References

Akiyama, S.K., Yamada, S.S., Chen, W.T., and Yamada, K.M. (1989). Analysis of fibronectin receptor function with monoclonal antibodies: Roles in cell adhesion, migration, matrix assembly, and cytoskeletal organization. J. Cell Biol. *109*, 863-875.

Arimori, T., Miyazaki, N., Mihara, E., Takizawa, M., Taniguchi, Y., Cabanas, C., Sekiguchi, K., and Takagi, J. (2021). Structural mechanism of laminin recognition by integrin. Nat Commun *12*, 4012.

Campbell, M.G., Cormier, A., Ito, S., Seed, R.I., Bondesson, A.J., Lou, J., Marks, J.D., Baron, J.L., Cheng, Y., and Nishimura, S.L. (2020). Cryo-EM Reveals Integrin-Mediated TGF-β Activation without Release from Latent TGF-β. Cell.

Chen, J.F., Salas, A., and Springer, T.A. (2003). Bistable regulation of integrin adhesiveness by a bipolar metal ion cluster. Nat. Struct. Biol. *10*, 995-1001.

Chen, J.F., Yang, W., Kim, M., Carman, C.V., and Springer, T.A. (2006). Regulation of outside-in signaling by the β2 I domain of integrin $\alpha_L\beta_2$. Proc. Natl. Acad. Sci. U. S. A. *103*, 13062-13067.

Dokmanic, I., Sikic, M., and Tomic, S. (2008). Metals in proteins: correlation between the metal-ion type, coordination number and the amino-acid residues involved in the coordination. Acta Crystallogr D Biol Crystallogr *64*, 257-263.

Dong, X., Zhao, B., Iacob, R.E., Zhu, J., Koksal, A.C., Lu, C., Engen, J.R., and Springer, T.A. (2017). Force interacts with macromolecular structure in activation of TGF-β. Nature *542*, 55-59.

Dransfield, I., Cabañas, C., Craig, A., and Hogg, N. (1992). Divalent cation regulation of the function of the leukocyte integrin LFA-1. J. Cell Biol. *116*, 219-226.

Gailit, J., and Ruoslahti, E. (1988). Regulation of the fibronectin receptor affinity by divalent cations. J Biol Chem *263*, 12927-12932.

Harding, M.M. (2001). Geometry of metal-ligand interactions in proteins. Acta Crystallogr D Biol Crystallogr *57*, 401-411.

Hu, D.D., Barbas III, C.F., and Smith, J.W. (1996). An allosteric Ca^{2+} binding site on the β3-integrins that regulates the dissociation rate for RGD ligands. J. Biol. Chem. *271*, 21745-21751.

Kechagia, J.Z., Ivaska, J., and Roca-Cusachs, P. (2019). Integrins as biomechanical sensors of the microenvironment. Nat Rev Mol Cell Biol *20*, 457-473.

Koivunen, E., Wang, B., and Ruoslahti, E. (1995). Phage libraries displaying cyclic peptides with different ring sizes: ligand specificities of the RGD-directed integrins. Biotechnology (N Y) *13*, 265-270.

Labadia, M.E., Jeanfavre, D.D., Caviness, G.O., and Morelock, M.M. (1998). Molecular regulation of the interaction between leukocyte function-associated antigen-1 and soluble ICAM-1 by divalent metal cations. J. Immunol. *161*, 836-842.

Lau, T.L., Kim, C., Ginsberg, M.H., and Ulmer, T.S. (2009). The structure of the integrin αIIbβ3 transmembrane complex explains integrin transmembrane signalling. EMBO J *9*, 1351-1361.

Lenter, M., Uhlig, H., Hamann, A., Jenö, P., Imhof, B., and Vestweber, D. (1993). A monoclonal antibody against an activation epitope on mouse integrin chain β_1 blocks adhesion of lymphocytes to the endothelial integrin $\alpha_6\beta_1$. Proc. Natl. Acad. Sci. U.S.A. *90*, 9051-9055.

Li, J., and Springer, T.A. (2017). Integrin extension enables ultrasensitive regulation by cytoskeletal force. Proc Natl Acad Sci U S A *114*, 4685-4690.

Li, J., and Springer, T.A. (2018). Energy landscape differences among integrins establish the framework for understanding activation. J Cell Biol *217*, 397-412.

Li, J., Su, Y., Xia, W., Qin, Y., Humphries, M.J., Vestweber, D., Cabanas, C., Lu, C., and Springer, T.A. (2017). Conformational equilibria and intrinsic affinities define integrin activation. EMBO J *36*, 629-645.

Lin, F.Y., Zhu, J., Eng, E., Hudson, N.E., and Springer, T.A. (2016). β-subunit binding is sufficient for ligands to open the integrin $\alpha_{IIb}\beta_3$ headpiece. J Biol Chem. *291*, 4537-4546.

Luo, B.H., Carman, C.V., and Springer, T.A. (2007). Structural basis of integrin regulation and signaling. Annu Rev Immunol *25*, 619-647.

Luque, A., Gomez, M., Puzon, W., Takada, Y., Sanchez-Madrid, F., and Cabanas, C. (1996). Activated conformations of very late activation integrins detected by a group of antibodies (HUTS) specific for a novel regulatory region (355-425) of the common β1 chain. J. Biol. Chem. *271*, 11067-11075.

Marlin, S.D., and Springer, T.A. (1987). Purified intercellular adhesion molecule-1 (ICAM-1) is a ligand for lymphocyte function-associated antigen 1 (LFA-1). Cell *51*, 813-819.

Miyake, K., Hasunuma, Y., Yagita, H., and Kimoto, M. (1992). Requirement for VLA-4 and VLA-5 integrins in lymphoma cells binding to and migration beneath stromal cells in culture. J. Cell Biol. *119*, 653-662.

Mould, A.P., Akiyama, S.K., and Humphries, M.J. (1995a). Regulation of integrin α5β1-fibronectin interactions by divalent cations. J. Biol. Chem. *270*, 26270-26277.

Mould, A.P., Askari, J.A., Barton, S., Kline, A.D., McEwan, P.A., Craig, S.E., and Humphries, M.J. (2002). Integrin activation involves a conformational change in the α1 helix of the β subunit A-domain. J. Biol. Chem. *277*, 19800-19805.

Mould, A.P., Barton, S.J., Askari, J.A., Craig, S.E., and Humphries, M.J. (2003a). Role of ADMIDAS cation-binding site in ligand recognition by integrin α5β1. J. Biol. Chem. *278*, 51622-51629.

Mould, A.P., Barton, S.J., Askari, J.A., McEwan, P.A., Buckley, P.A., Craig, S.E., and Humphries, M.J. (2003b). Conformational changes in the integrin βA domain provide a mechanism for signal transduction via hybrid domain movement. J Biol Chem *278*, 17028-17035.

Mould, A.P., Garratt, A.N., Askari, J.A., Akiyama, S.K., and Humphries, M.J. (1995b). Identification of a novel anti-integrin monoclonal antibody that recognises a ligand-induced binding site epitope on the β1 subunit. FEBS Lett. *363*, 118-122.

Mould, A.P., Travis, M.A., Barton, S.J., Hamilton, J.A., Askari, J.A., Craig, S.E., Macdonald, P.R., Kammerer, R.A., Buckley, P.A., and Humphries, M.J. (2005). Evidence that monoclonal antibodies directed against the integrin β subunit plexin/semaphorin/integrin domain stimulate function by inducing receptor extension. J. Biol. Chem. *280*, 4238-4246.

Nagae, M., Re, S., Mihara, E., Nogi, T., Sugita, Y., and Takagi, J. (2012). Crystal structure of $\alpha_5\beta_1$ integrin ectodomain: Atomic details of the fibronectin receptor. J Cell Biol *197*, 131-140.

Schumacher, S., Dedden, D., Nunez, R.V., Matoba, K., Takagi, J., Biertumpfel, C., and Mizuno, N. (2021). Structural insights into integrin α5β1 opening by fibronectin ligand. Sci Adv *7*.

Speight, J. (2016). Lange's Handbook of Chemistry. McGraw Hill.

Springer, T.A., and Dustin, M.L. (2012). Integrin inside-out signaling and the immunological synapse. Curr. Opin. Cell Biol. *24*, 107-115.

Springer, T.A., Zhu, J., and Xiao, T. (2008). Structural basis for distinctive recognition of fibrinogen γC peptide by the platelet integrin $\alpha_{IIb}\beta_3$. J. Cell Biol. *182*, 791-800.

Staatz, W.D., Rajpara, S.M., Wayner, E.A., Carter, W.G., and Santoro, S.A. (1989). The membrane glycoprotein Ia-IIa (VLA-2) complex mediates the Mg^{2+}-dependent adhesion of platelets to collagen. J. Cell Biol. *108*, 1917-1924.

Su, Y., Xia, W., Li, J., Walz, T., Humphries, M.J., Vestweber, D., Cabañas, C., Lu, C., and Springer, T.A. (2016). Relating conformation to function in integrin α5β1. Proc Natl Acad Sci U S A. *113*, E3872-3881.

Sun, Z., Costell, M., and Fassler, R. (2019). Integrin activation by talin, kindlin and mechanical forces. Nat Cell Biol *21*, 25-31.

Takagi, J., Petre, B.M., Walz, T., and Springer, T.A. (2002). Global conformational rearrangements in integrin extracellular domains in outside-in and inside-out signaling. Cell *110*, 599-611.

Valdramidou, D., Humphries, M.J., and Mould, A.P. (2008). Distinct roles of β1 metal ion-dependent adhesion site (MIDAS), adjacent to MIDAS (ADMIDAS), and ligand-associated metal-binding site (LIMBS) cation-binding sites in ligand recognition by integrin α2β1. J Biol Chem *283*, 32704-32714.

Wang, J., Su, Y., Iacob, R.E., Engen, J.R., and Springer, T.A. (2019). General structural features that regulate integrin affinity revealed by atypical αVβ8. Nat Commun *10*, 5481.

Xiao, T., Takagi, J., Wang, J.-H., Coller, B.S., and Springer, T.A. (2004). Structural basis for allostery in integrins and binding of fibrinogen-mimetic therapeutics. Nature *432*, 59-67.

Xiong, J.-P., Stehle, T., Diefenbach, B., Zhang, R., Dunker, R., Scott, D.L., Joachimiak, A., Goodman, S.L., and Arnaout, M.A. (2001). Crystal structure of the extracellular segment of integrin αVβ3. Science *294*, 339-345.

Xiong, J.P., Stehle, T., Zhang, R., Joachimiak, A., Frech, M., Goodman, S.L., and Arnaout, M.A. (2002). Crystal structure of the extracellular segment of integrin $\alpha_V\beta_3$ in complex with an Arg-Gly-Asp ligand. Science *296*, 151-155.

Ye, F., Kim, C., and Ginsberg, M.H. (2012). Reconstruction of integrin activation. Blood *119*, 26-33.

Zhu, J., Choi, W.-S., McCoy, J.G., Negri, A., Zhu, J., Naini, S., Li, J., Shen, M., Huang, W., Bougie, D., Rasmussen, M., Aster, R., Thomas, C.J., Filizola, M., Springer, T.A., and Coller, B.S. (2012). Structure-guided design of a high affinity platelet integrin $\alpha_{IIb}\beta_3$ receptor antagonist that disrupts Mg^{2+} binding to the MIDAS. Sci. Transl. Med. *4*, 125-132.

Zhu, J., Luo, B.H., Barth, P., Schonbrun, J., Baker, D., and Springer, T.A. (2009). The structure of a receptor with two associating transmembrane domains on the cell surface: integrin αIIbβ3. Mol. Cell *34*, 234-249.

Zhu, J., Zhu, J., and Springer, T.A. (2013). Complete integrin headpiece opening in eight steps. J. Cell Biol. *201*, 1053-1068.

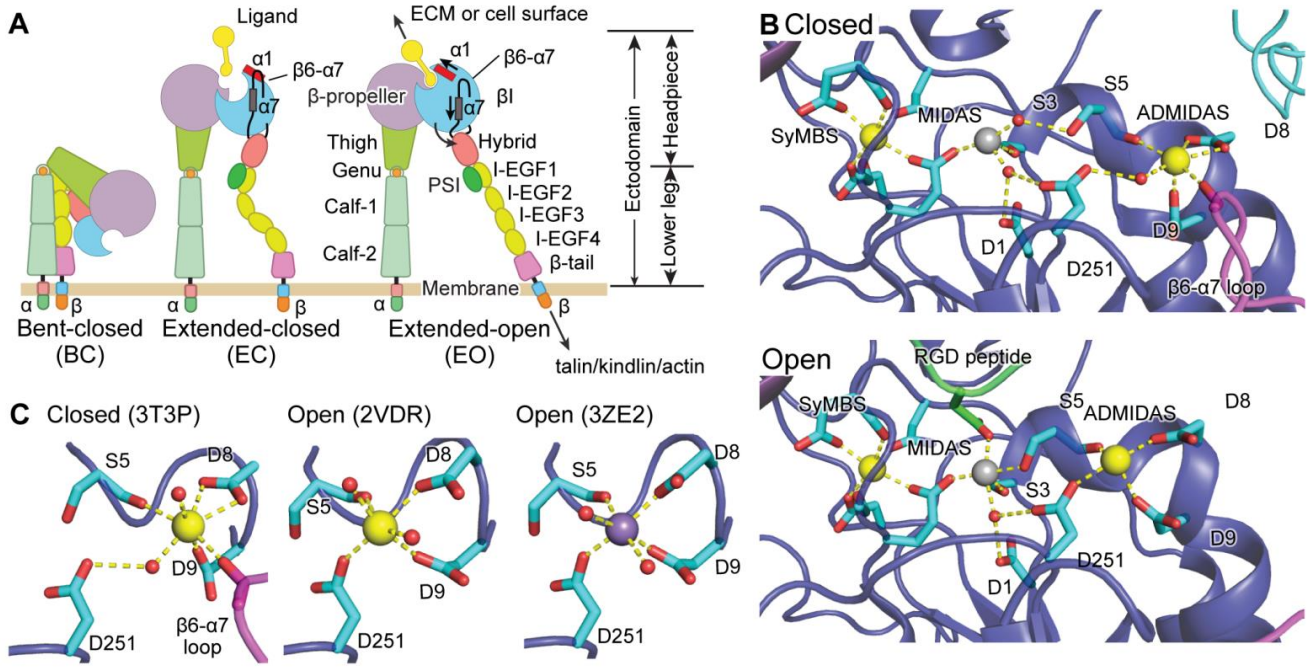

D

	State(s)	K_a^{Ens} for ligand	Fab(s)
(Eq.1)	BC+EC+EO	$K_a^{Ens\,(Basal)} = P^{BC}+K_a^{BC}+P_a^{EC}+K_a^{EC}$	None
(Eq.2)	EC+EO	$K_a^{Ens\,(EC+EO)} = \frac{P^{EC}}{P^{EC}+P^{EO}} K_a^{EC} + \frac{P^{EO}}{P^{EC}+P^{EO}} K_a^{EO}$	8E3; 9EG7
(Eq.3)	BC+EC	$K_a^{Ens\,(BC+EC)} = \frac{P^{BC}}{P^{BC}+P^{EC}} K_a^{BC} + \frac{P^{EC}}{P^{BC}+P^{EC}} K_a^{EC}$	mAb13
	EO	K_a^{EO}	12G10; HUTS4; 9EG7 & HUTS4

E

Fab	Domain	Conformational specificity	States
HUTS4	hybrid	Open	EO
12G10	βI	Open	EO
9EG7	I-EGF2	Extended	EC+EO
8E3	PSI	Extended	EC+EO
SG/19	βI/hybrid	Closed	BC+EC
mAb13	βI	Closed	BC+EC

Figure Legend.

Figure 1. Integrin conformational states and their equilibria. (**A**) Domain organization and conformational states of integrin α5β1. The α1-helix, α7-helix and β6-α7 loop that move during opening of the βI domain are labeled. ECM: extracellular matrix. (**B**) Details around the βI domain metal ion binding sites of closed and liganded, open conformations. (**C**) The coordination number of the ADMIDAS in the closed state is 7 and in the open state is 6. **B** and **C** use integrin αIIbβ3, for which high resolution closed and open structures are available. Closed: PDB 3T3P (Zhu *et al.*, 2012), open: PDB 2VDR (Springer *et al.*, 2008) and PDB 3ZE2, chain D with a soaked-in Mn^{2+} ion (Zhu *et al.*, 2013). Physiologically, the SyMBS and ADMIDAS are occupied by Ca^{2+} (gold spheres) while the MIDAS is occupied by Mg^{2+} (silver sphere). Mn^{2+} is shown as a violet sphere. β-MIDAS residues (D1-S3-S5-D8-D9) and other coordinating residues are shown with cyan carbons in stick, except the β6-α7 loop and its carbonyl are shown in magenta. The RGD Asp is shown as green. Oxygens are shown in red. Small red spheres are water molecules, except one oxygen in 3ZE2 is from a glycerol molecule used as cryoprotectant. (**D**) Equation 1 relates the basal ensemble affinity ($K_d^{ens(Basal)}$) to the affinities of the BC (K_d^{BC}), EC (K_d^{EC}) and EO (K_d^{EO}) states with the populations of these states (P^{BC}, P^{EC} and P^{EO} respectively). Equations 2 and 3 show how the affinity of the extended ($K_d^{Ens(EO+EC)}$) and closed ($K_d^{Ens(EC+BC)}$) ensemble are described (Li *et al.*, 2017). Listed to the right are the Fabs that are specific for and stabilize these states or ensembles. (**E**) The domain and conformational specificities of the Fabs used here.

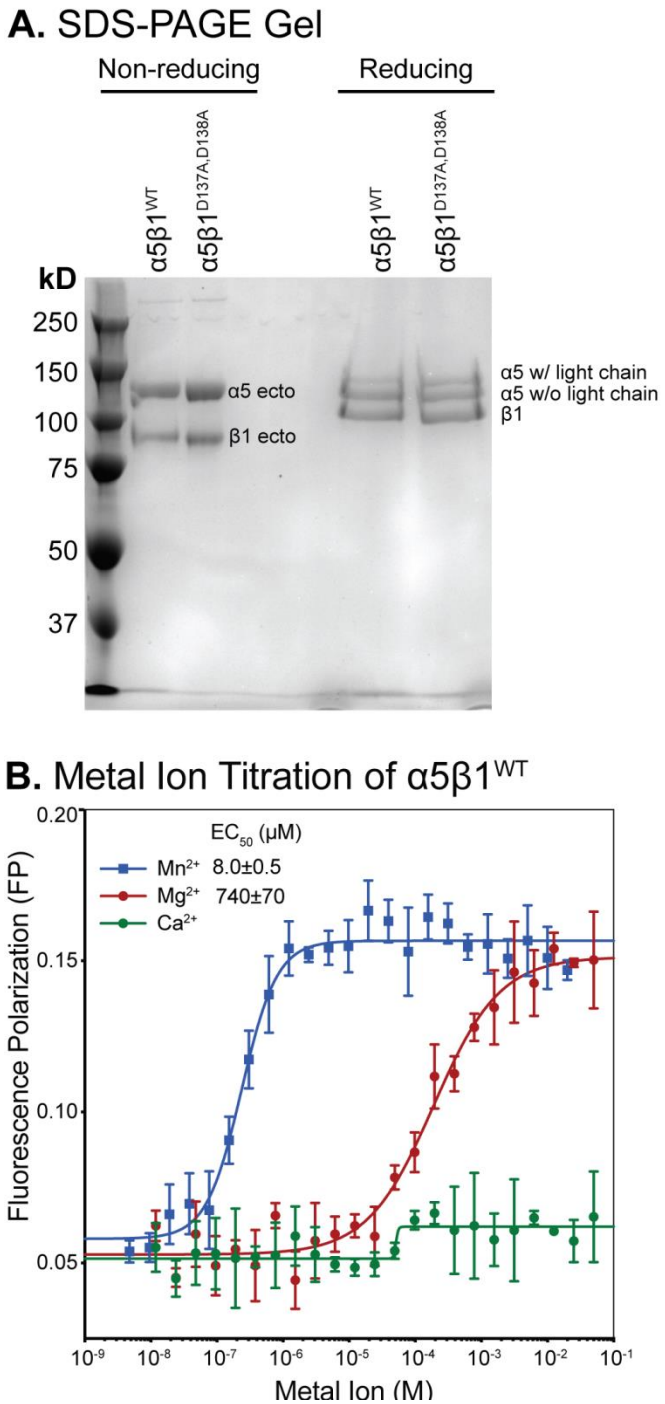

Figure 2. Integrin preparations and metal ion effects on α5β1^{WT}. (**A**) SDS-PAGE (7.5% polyacrylamide) of α5β1^{WT} and α5β1$^{D137A, D138A}$ in non-reducing and reducing conditions. The α5 chain is divided into two disulfide-linked fragments by furin cleavage. (**B**) FP assay showing the effect of metal ions on the binding of α5β1^{WT} (20 nM) to FITC-cRGD peptide (5 nM) in pH 7.4 TBS. Titrations were done in triplicate.

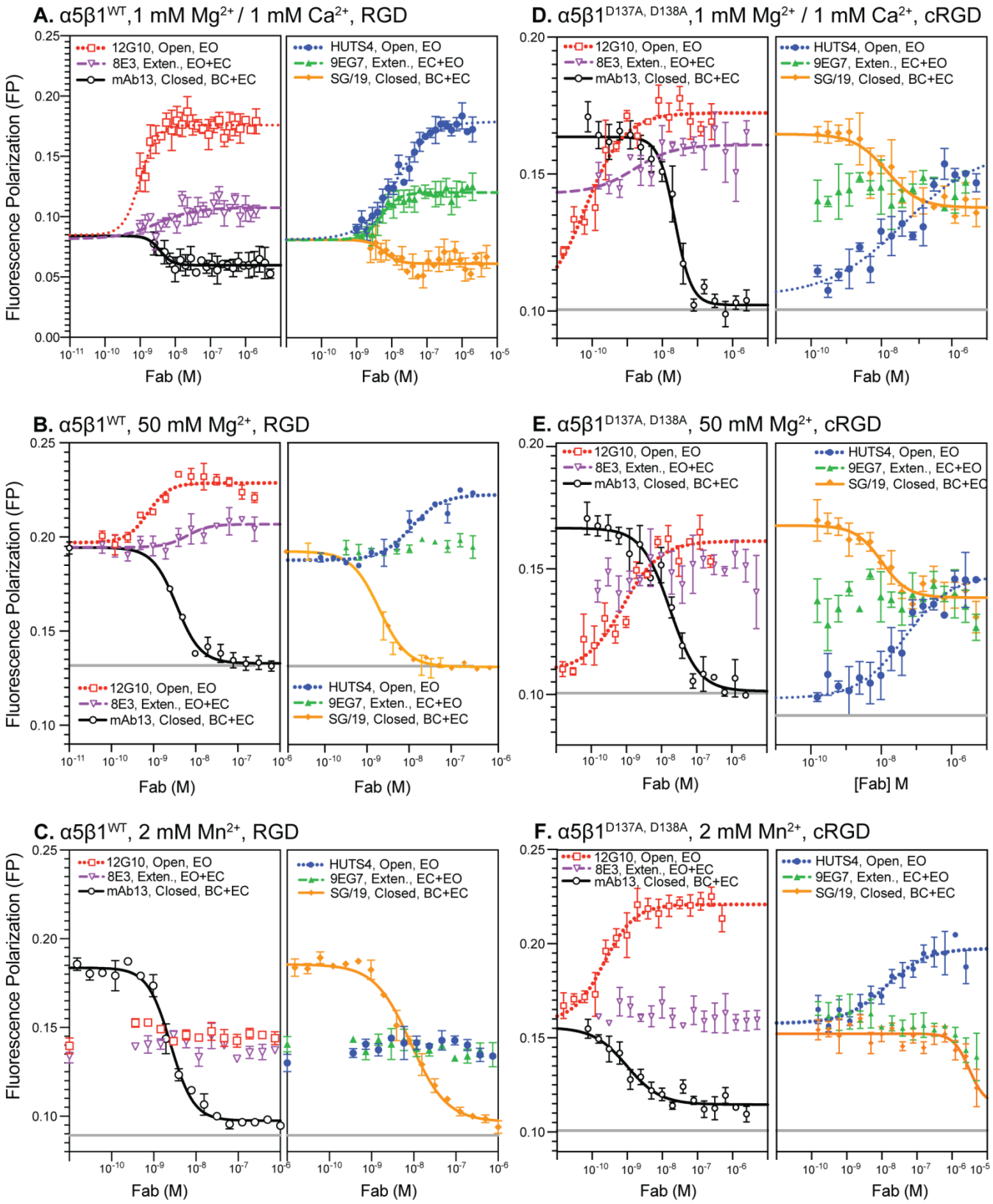

Figure 3. **Impact of increasing Fab concentration on the binding of FITC-RGD peptide for α5β1^{WT} and α5β1$^{D137A, D138A}$ ectodomain.** To determine saturating concentrations of Fabs for each metal ion condition, used later in experiments to measure the intrinsic affinities of the extended-open state and extended and closed ensembles, Fabs were titrated in the presence of a constant concentration of (**A-**

C) α5β1^{WT} or (**D-F**) α5β1$^{D137A, D138A}$ ectodomain and RGD ligand (FITC-RGD for α5β1^{WT} and FITC-cRGD for α5β1$^{D137A, D138A}$). EC_{50} values for each titration are summarized in Table S1. Concentrations of integrin and ligand used in each titration are summarized in Table S2. Fab titrations of α5β1^{WT} ectodomain in physiological conditions (A, 1mM Mg^{2+}/1 mM Ca^{2+}) were previously reported (Li *et al.*, 2017). Fitting curves are not shown for datasets where the fitting error (SE) is comparable to or greater than the fitted value of the parameter. Titrations were done in triplicate.

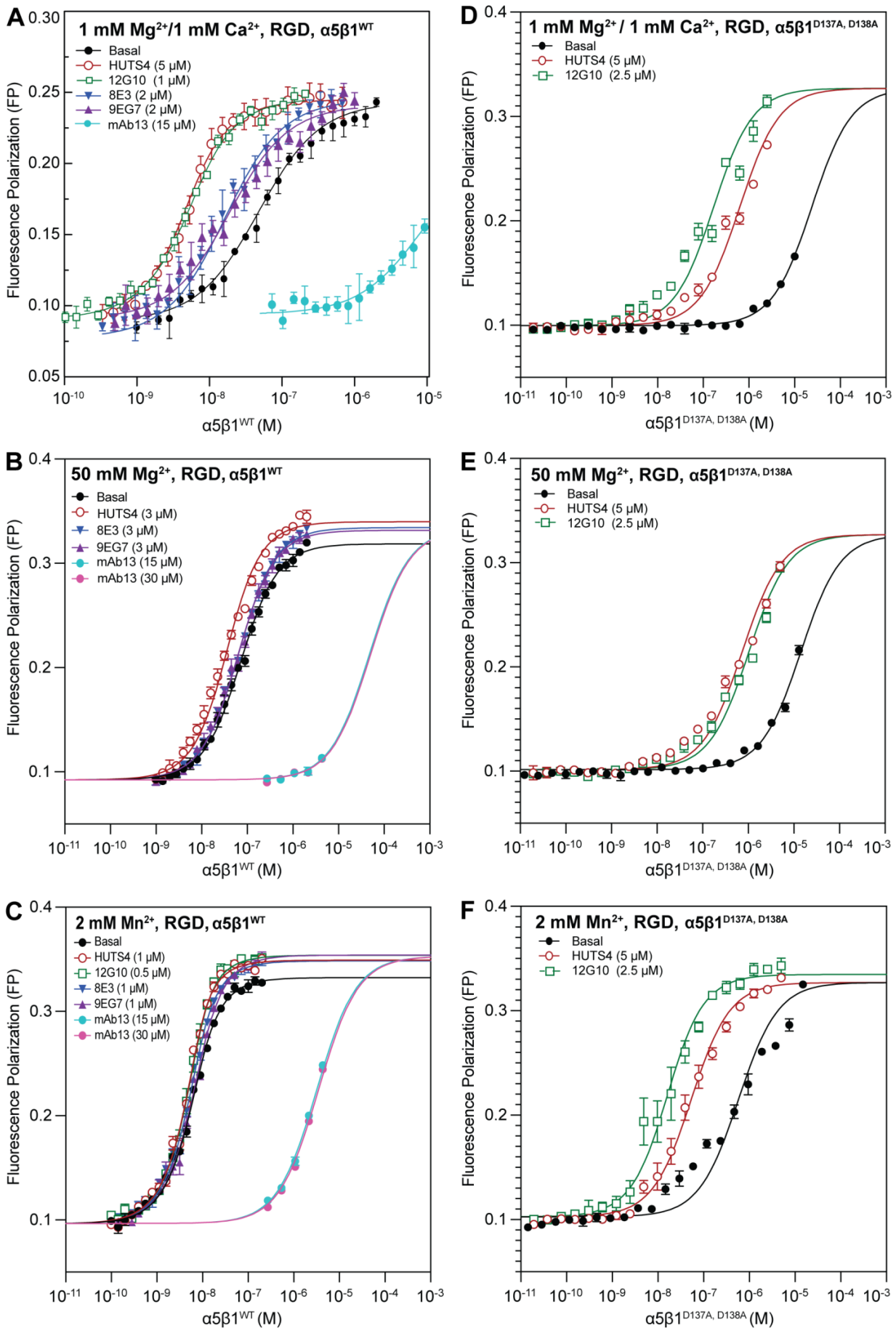
A
1 mM Mg2+/1 mM Ca2+, RGD, α5β1WT
Basal
HUTS4 (5 μM)
12G10 (1 μM)
8E3 (2 μM)
9EG7 (2 μM)
mAb13 (15 μM)
Fluorescence Polarization (FP)
α5β1WT (M)
B
50 mM Mg2+, RGD, α5β1WT
Basal
HUTS4 (3 μM)
8E3 (3 μM)
9EG7 (3 μM)
mAb13 (15 μM)
mAb13 (30 μM)
Fluorescence Polarization (FP)
α5β1WT (M)
C
2 mM Mn2+, RGD, α5β1WT
Basal
HUTS4 (1 μM)
12G10 (0.5 μM)
8E3 (1 μM)
9EG7 (1 μM)
mAb13 (15 μM)
mAb13 (30 μM)
Fluorescence Polarization (FP)
α5β1WT (M)
D
1 mM Mg2+ / 1 mM Ca2+, RGD, α5β1D137A, D138A
Basal
HUTS4 (5 μM)
12G10 (2.5 μM)
Fluorescence Polarization (FP)
α5β1D137A, D138A (M)
E
50 mM Mg2+, RGD, α5β1D137A, D138A
Basal
HUTS4 (5 μM)
12G10 (2.5 μM)
Fluorescence Polarization (FP)
α5β1D137A, D138A (M)
F
2 mM Mn2+, RGD, α5β1D137A, D138A
Basal
HUTS4 (5 μM)
12G10 (2.5 μM)
Fluorescence Polarization (FP)
α5β1D137A, D138A (M)

Figure 4. Ensemble and intrinsic affinities of α5β1^{WT} and α5β1$^{D137A, D138A}$ ectodomain for FITC-RGD. Basal ensemble and intrinsic affinities of both α5β1^{WT} (**A-C**) and α5β1$^{D137A, D138A}$ ectodomain (**D-F**) for FITC-RGD were determined in the presence of 1 mM Mg^{2+} / 1 mM Ca^{2+}, 50 mM Mg^{2+}, and 2 mM Mn^{2+}. Intrinsic affinities of the open (EO, 12G10 and HUTS4), extended (EO+EC, 9EG7 and 8E3), and closed (EC+BC, mAb13) ensembles were determined by titrating integrin in the presence of FITC-RGD (5 nM) and saturating concentration of Fab. The concentration of Fab used in each titration can be found in each graph legend. (A) The titrations of α5β1^{WT} ectodomain in 1 mM Mg^{2+}/1 mM Ca^{2+} were previously reported in Li et al. (Li *et al.*, 2017). All assays also contain pH 7.4, 20 mM Tris, 150 mM NaCl. Fitted Affinities (K_d) are reported in Table S3. The titrations shown were done in triplicate, and basal ensemble affinities (panels of B and C) were measured three times (averaged in Table 1).

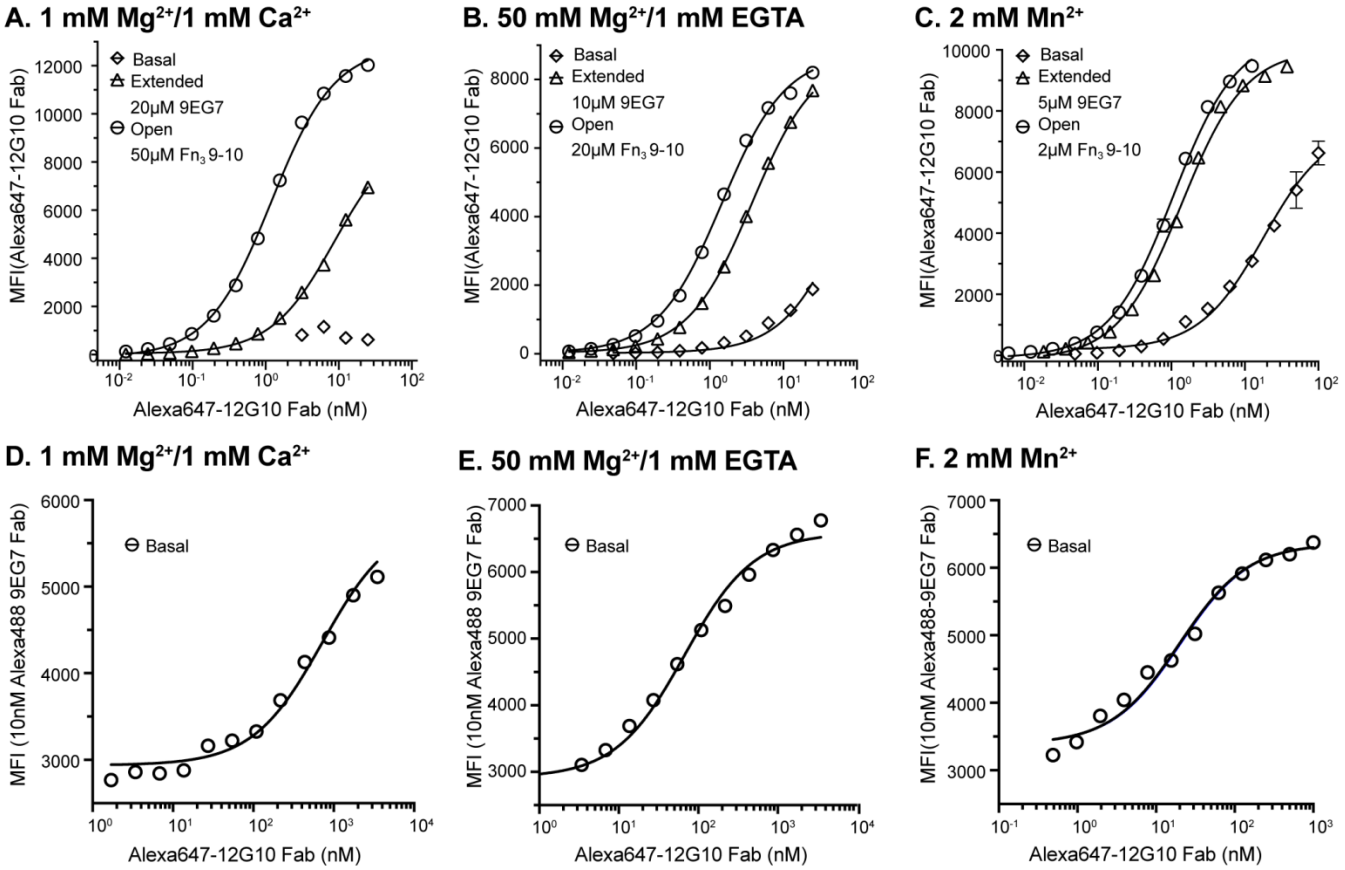

G.

	State(s)	Allosteric stabilizers	$K^{ens}_{a,12G10}$
(Eq.4)	BC+EC+EO	None	$K^{ens\,(Basal)}_{a,12G10} = \frac{P^{EO}}{P^{BC}+P^{EC}+P^{EO}} K^{EO}_{a,12G10}$
(Eq.5)	EC+EO	9EG7	$K^{ens\,(EC+EO)}_{a,12G10} = \frac{P^{EO}}{P^{EC}+P^{EO}} K^{EO}_{a,12G10}$
	EO	$Fn_3$9-10	$K^{EO}_{a,12G10}$

H. Energy landscape of α5β1 on K562 cell surface derived from affinity of Alexa647-12G10 Fab

Cations	1 mM Mg^{2+}/1 mM Ca^{2+}	50 mM Mg^{2+}/1 mM EGTA	2 mM Mn^{2+}
$K^{ens(Basal)}_{d,12G10}$ (nM)	750±105	67±8#	17.4±2.4#
$K^{ens(EC+EO)}_{d,12G10}$ (nM)	8.7±0.5	3.6±0.1	1.2±0.1
$K^{EO}_{d,12G10}$ (nM)	1.0±0.1	1.2±0.1	0.9±0.1
P^{BC} (%)	98.8±0.2	94.6±0.7	93.1±1.1
P^{EC} (%)	1.0±0.1	3.6±0.5	2.0±0.7
P^{EO} (%)	0.13±0.02	1.8±0.3	4.9±0.7
ΔG^{BC} (kcal/mol)	−3.9±0.1	−2.3±0.1	−1.7±0.1
ΔG^{EC} (kcal/mol)	-1.2±0.1	-0.4±0.1	0.5±0.1

Error is reported as the difference from the mean of the basal ensemble affinities determined in panels B and E, or panels C and F.

Figure 5. Influence of cations on the conformational equilibrium of intact α5β1^{WT}. (A-C) Binding of Alexa647-labelled 12G10 Fab for defined intact α5β1^{WT} ensembles under 1 mM Mg^{2+}/1 mM Ca^{2+} (A), 50 mM Mg^{2+}/1 mM EGTA (B), and 2 mM Mn^{2+} (C) by flow cytometry without washing. The concentration of 9EG7 Fab to saturably stabilize the two extended states and Fn3 9-10 to saturably stabilize the EO state under each cation condition was determined in Figure S2. Background subtracted mean fluorescence intensity (MFI) as a function of Alexa647-12G10 Fab concentration was fitted to dose response curve for the K_d of 12G10 Fab for the different ensembles. (**D-F**) Enhancement of 10 nM Alexa488-labelled 9EG7 Fab binding to K562 cells by increasing Alexa647-12G10 Fab concentration under 1 mM Mg^{2+}/1 mM Ca^{2+} (D), 50 mM Mg^{2+}/1 mM EGTA (E), and 2 mM Mn^{2+} (F) by flow cytometry without washing. MFI of 10 nM Alexa488-labelled 9EG7 Fab at different Alexa647-12G10 Fab concentrations were fitted to dose response curve for K_d values of 12G10 Fab for the basal ensemble. (G) The equations used to calculate the population of each conformational state from the affinities of Alexa647-12G10 Fab measured for the defined ensembles. (**H**) Tabulations of Alexa647-12G10 affinities determined for the defined ensembles, as well as the population of each conformational state

calculated with Eq.4 and Eq.5 shown in Panel G, and the free energies of BC and EC state relative to EO state calculated from these populations based on Boltzmann distribution.

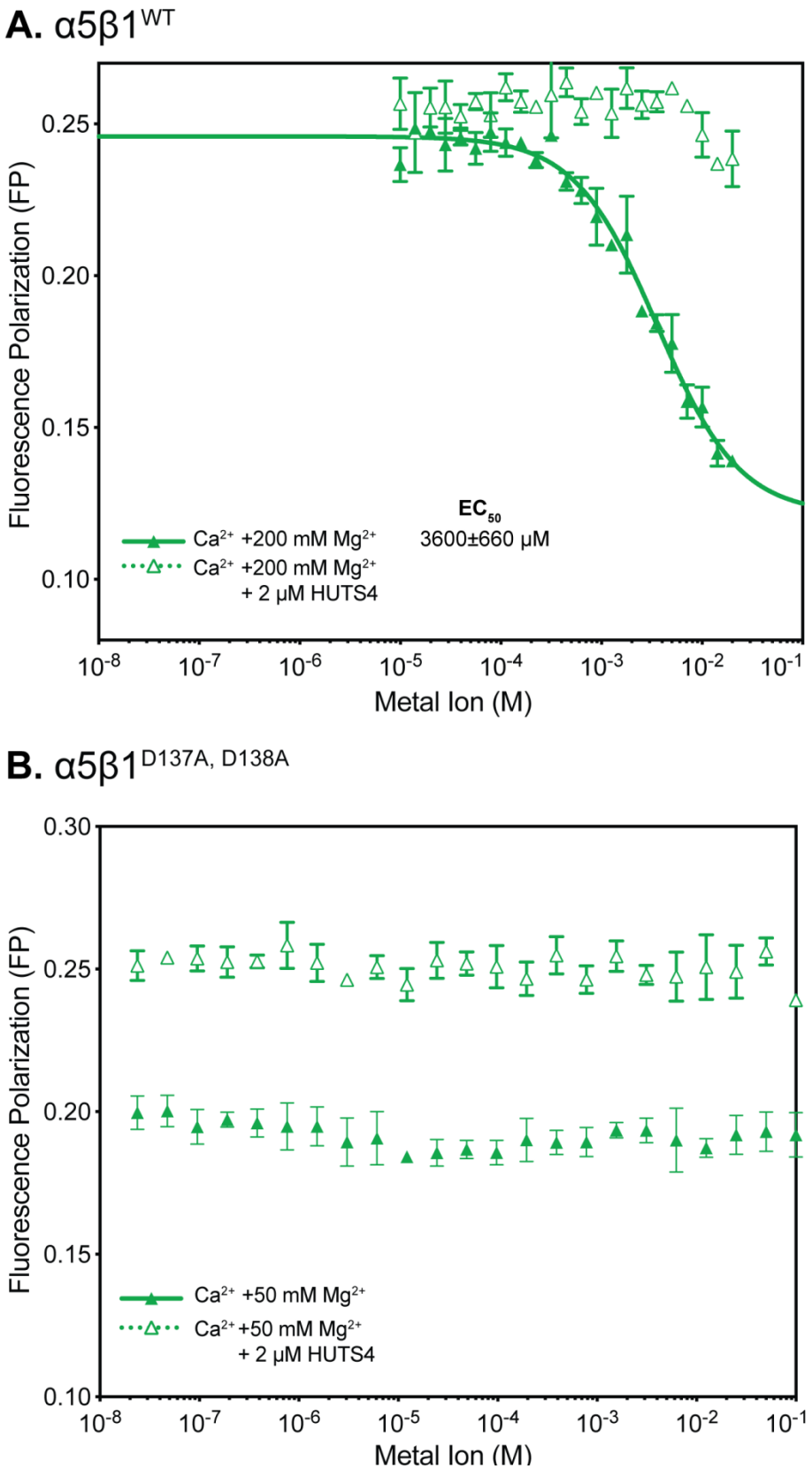

Figure 6. Metal ion EC_{50} values for $\alpha5\beta1^{WT}$ and $\alpha5\beta1^{D137A, D138A}$ and inhibition by Ca^{2+} at the ADMIDAS. In FP assays containing 5 nM FITC-cyclic RGD peptide in the absence or presence of open-stabilizing HUTS4 Fab, Mg^{2+} alone was titrated or Ca^{2+} was titrated in the presence of saturating

concentrations of Mg^{2+} with (**A**) 20 nM α5β1^{WT} or (**B**) 200 nM α5β1$^{D137A, D138A.}$ Buffer was 20 mM Tris-HCL pH 7.4, 150 mM NaCl. Each point was in triplicate. Fit lines are shown only when fit values were greater or similar to the fit error.

Table 1. α5β1 ectodomain ensemble affinities and populations[a]

Ligand		α5β1 WT			α5β1 D137A, D138A		
		1 mM Mg^{2+} 1 mM Ca^{2+}	50 mM Mg^{2+}	2 mM Mn^{2+}	1 mM Mg^{2+} 1 mM Ca^{2+}	50 mM Mg^{2+}	2 mM Mn^{2+}
RGD	$K_d^{ens(Basal)}$ (nM)	2,300±800[b]	63±4[c]	3.9±0.6[c]	24000±3600[f]	14000±1300[f]	580±62[f]
	$K_d^{ens(EC+EO)}$ (nM)	620±50[b]	54±3[f,i]	2.8±0.3[f,i]	-	-	-
	$K_d^{ens(BC+EC)}$ (nM)	≥220,000[b,e]	49,000±9000[f,j]	3,300±130[f,j]	-	-	-
	K_d^{EO} (nM)	71±5[b]	26±2[f,k]	1.6±0.2[f,k]	170±14[f,l]	1000±76[f,l]	14±2[f,l]
	P^{BC} (%)	73.2±9.6[b]	14.3±7.2	28.2±13.5	-	-	-
	P^{EC} (%)	23.7±8.7[b]	44.5±6.4	30.8±10.4	-	-	-
	P^{EO} (%)	3.1±1.1[b]	41.2±4.1	41.0±8.1	-	-	-
	ΔG^{BC} (kcal/mol)	-1.8±0.3[b]	0.62±0.3	0.22±0.4	-	-	-
	ΔG^{EC} (kcal/mol)	-1.2±0.1[b]	-0.04±0.1	0.17±0.2	-	-	-
cRGD	$K_d^{ens(Basal)}$ (nM)	47±3[b]	1.6±0.1[g]	0.20±0.05[g]	65±49[d]	76±4[c]	2.5±2[c]
	$K_d^{ens(BC+EC)}$ (nM)	7000±3400[b]	1500±200[g]	46±5[g]	770±150[h]	1200±13[h,j]	14±0.7[h,j]

[a] Values are ± fitting errors, unless footnoted[c,d].
[b] Previously reported {Li, 2017 #24745}
[c] Average of three experiments. Errors (±) are standard deviations between independent experiments.
[d] Average of five experiments. Errors (±) are standard deviations between independent experiments.
[e] 220,000 nM was estimated from the intrinsic affinity fold difference between the BC+EC and the EO states for multiple RGD ligands. 600,000 nM was estimated from the sensitivity of the RGD binding assay in Fig. 4A of {Li, 2017 #24745}.
[f] Titrations in Figure 4
[g] Titrations in Figure S1
[h] Titrations in Figure S5
[i] Affinity averaged from titrations in the presence of 9EG7 and 8E3
[j] Affinity averaged from titrations in the presence of mAb13.
[k] Affinity averaged from titrations in the presence of 12G10 and HUTS4
[l] Affinity from titrations in the presence of 12G10

Supplementary Materials

Molecular Biology of the Cell

Anderson *et al.*

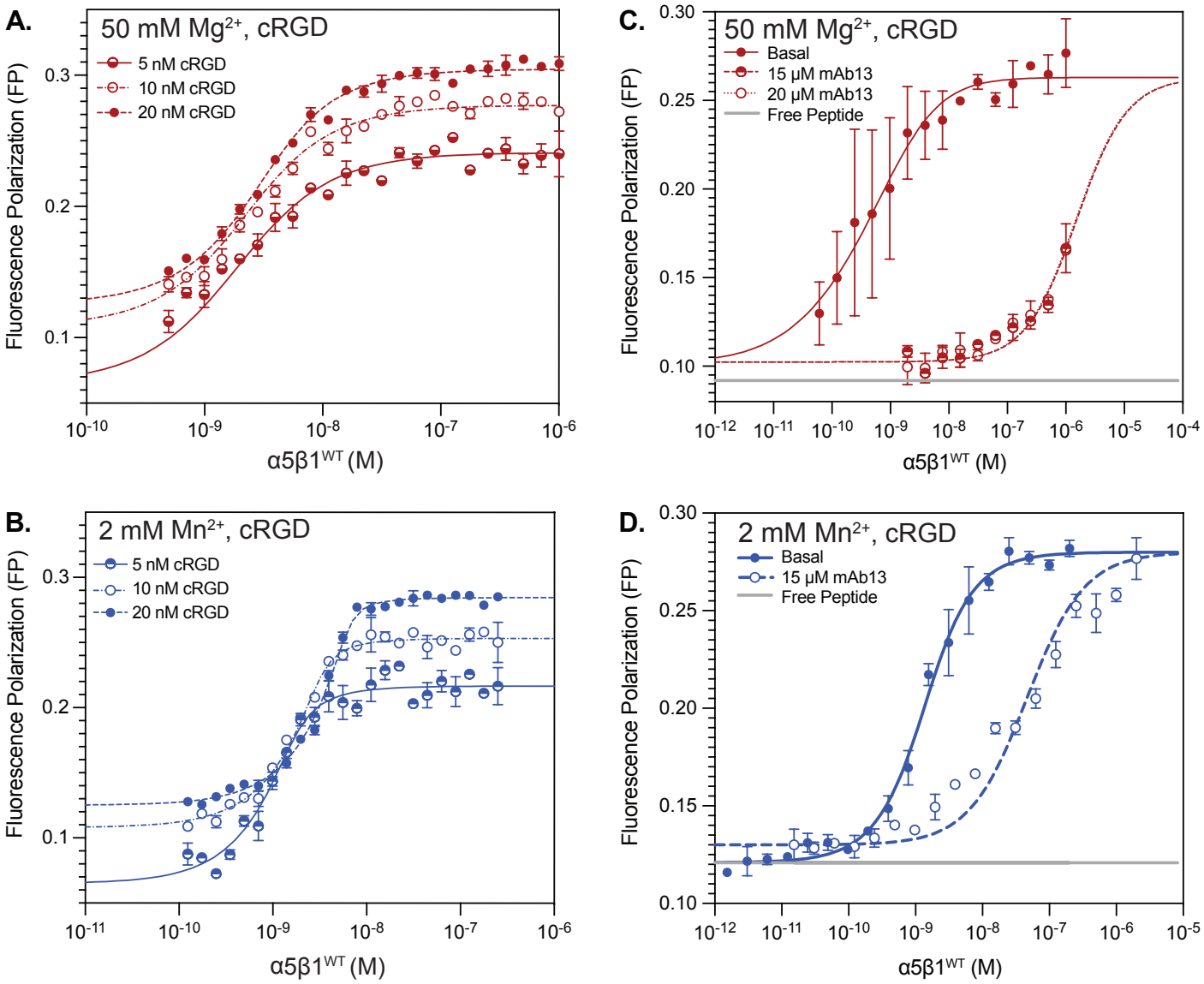

Figure S1. Affinities of α5β1^{WT} for FITC-cRGD. (A-B) α5β1^{WT} was titrated in the presence of FITC-cRGD peptide at three concentrations in (A) 50 mM Mg^{2+} (red) and (B) 2 mM Mn^{2+} (blue). Multiple concentrations of ligand are used to compensate for ligand depletion effects at affinities >1 nM by globally fitting K_d values. (C-D) The closed ensemble (EC+BC) of α5β1^{WT} for ligand FITC-cRGD in (C) 50 mM Mg^{2+} and (D) 2 mM Mn^{2+} was measured by titrating α5β1^{WT} in absence (basal, solid line) and presence of mAb13 fab (15 and 20 μM, dashed and dotted respectively), with 10 nM FITC-cRGD peptide. All titrations contain pH 7.4 TBS. Titrations were done in triplicate and fitted affinities are shown in Table 1.

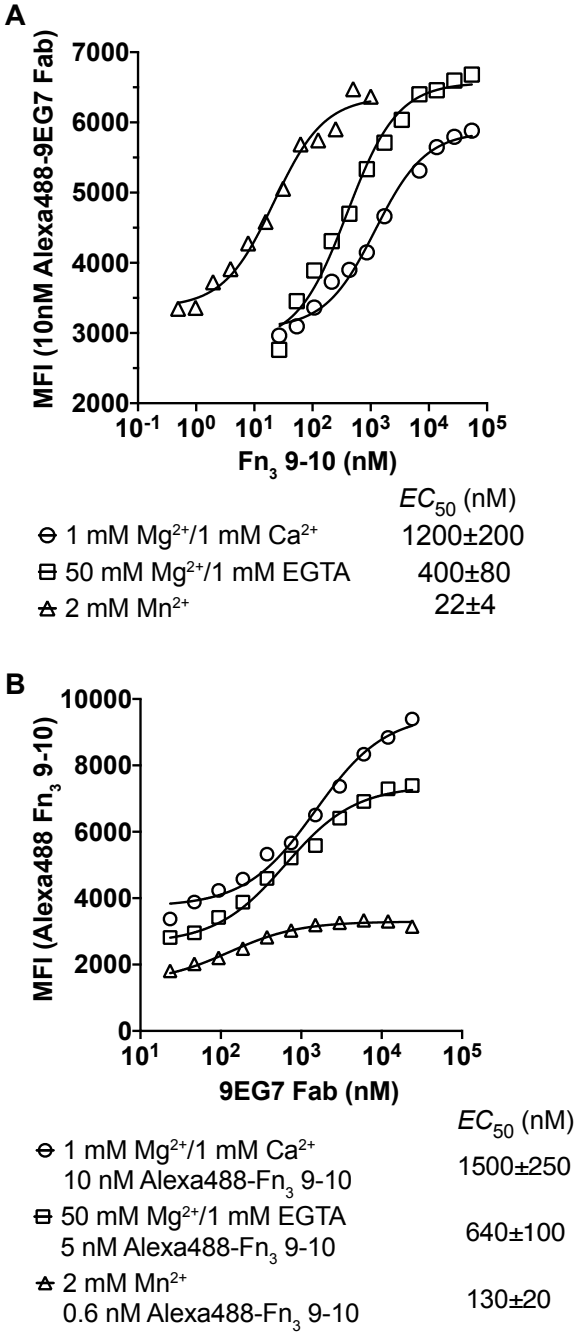

Figure S2. Titrations of intact α5β1^{WT} on K562 cells with Fn_3 9-10 and Fab 9EG7. Concentrations necessary to saturate intact α5β1 on K562 cells with Fn_3 9-10 and Fab 9EG7, for use in determining the conformational landscape of cell-bound α5β1 in the conditions of 1 mM Mg^{2+}/1 mM Ca^{2+}, 50 mM Mg^{2+}/1 mM EGTA, and 2 mM Mn^{2+}. (A and B) Alexa488-9EG7 Fab (10 nM) (A) or Alexa488-$Fn_3$9-10 (10, 5, or 0.6 nM as indicated) (B) binding to K562 cells (2 × 10^6 cells/ml) was measured by FACS, without washing, in presence of unlabeled Fn_3 9-10 (A) or 9EG7 Fab (B).

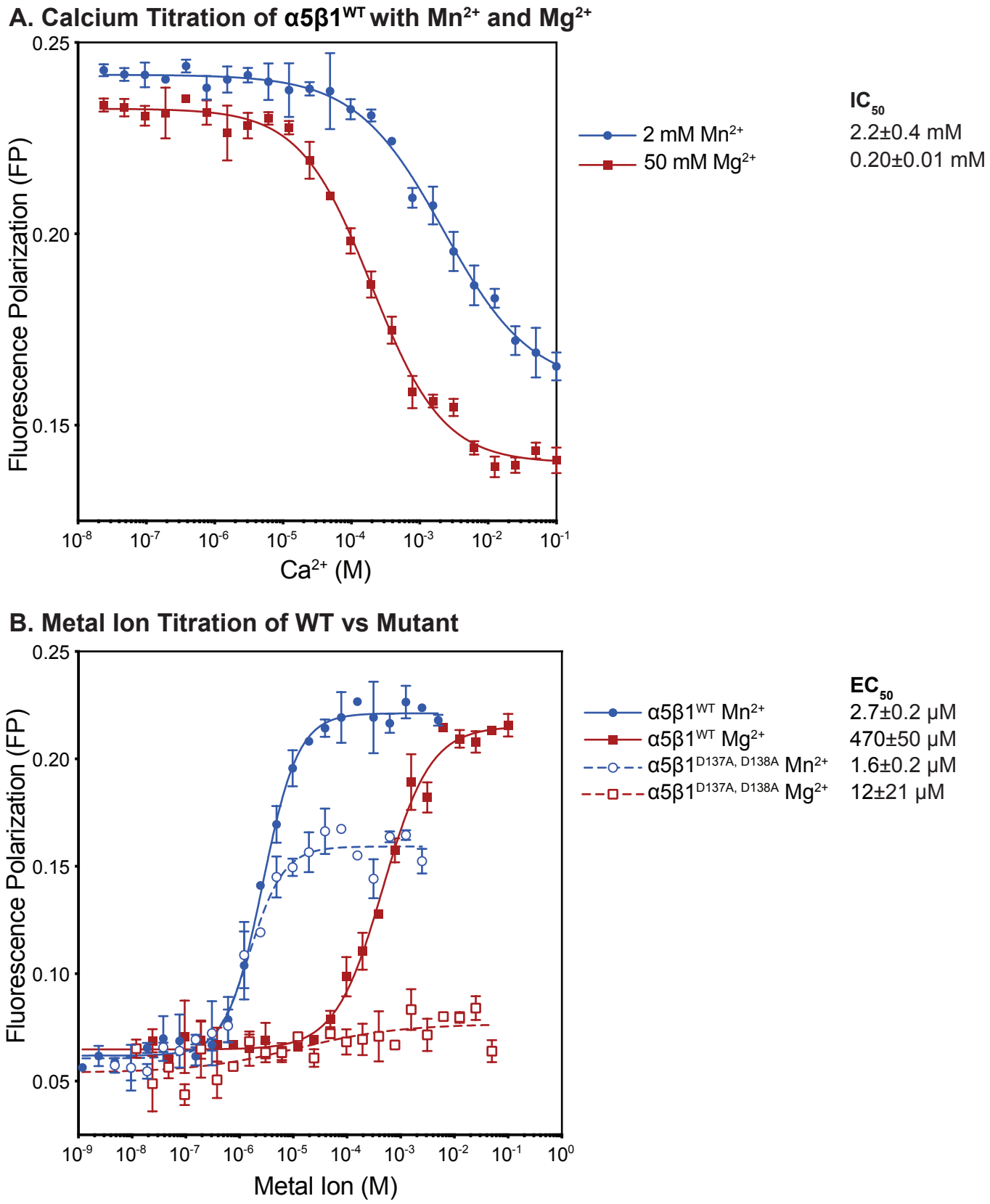

Figure S3. Metal Ion titrations of α5β1. (A) Inhibition by calcium of binding of α5β1^{WT} (20 nM) to FITC-cRGD (5 nM) in 2 mM Mn^{2+} (blue) or 50 mM Mg^{2+} (red). (B) α5β1$^{D137A, D138A}$ shows a reduced FP signal during titration with Mn^{2+} and Mg^{2+} compared to α5β1^{WT}, because of the lower affinity α5β1$^{D137A, D138A}$ has for FITC-cRGD. α51^{WT} (solid lines, 20 nM) and α5β1$^{D137A, D138A}$ (dashed lines, 20 nM) were titrated with Mn^{2+} (blue) or Mg^{2+}(red) in the presence of FITC-cRGD (5 nM). This experiment also shows that 2 mM Mn^{2+} is saturating for both α5β1^{WT} and α5β1$^{D137A, D138A}$. Titrations were done in triplicate.

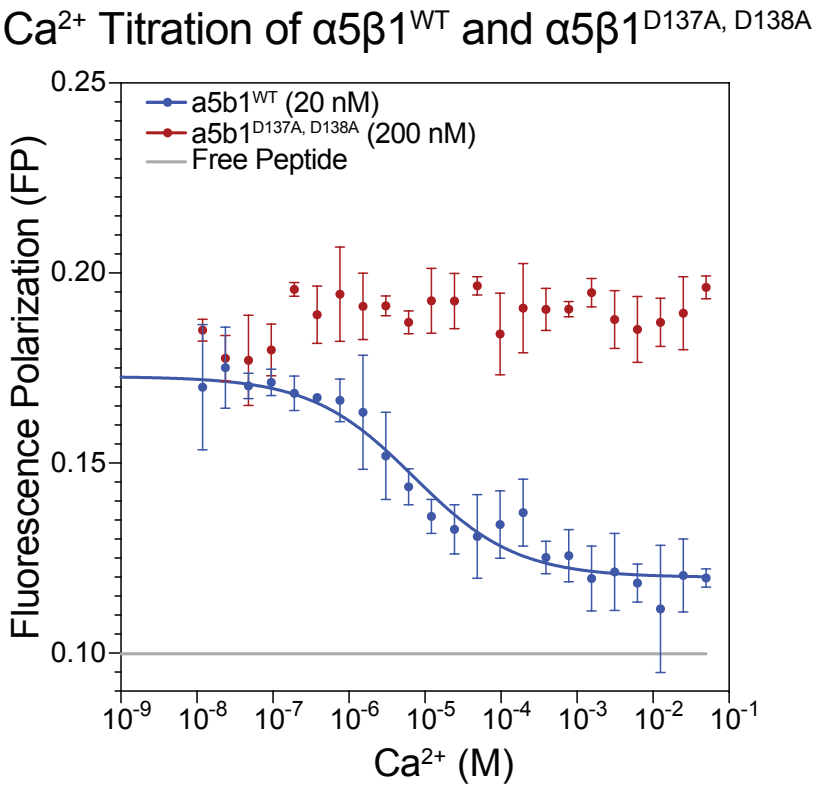

Figure S4. Calcium ion titrations of α5β1^{WT} and α5β1$^{D137A, D138A}$ in 1 mM Mg^{2+}. Similar to Fig. 6, α5β1^{WT} and α5β1$^{D137A, D138A}$ were titrated with Ca^{2+}, in the presence of 1 mM Mg^{2+}. It was found that while binding of α5β1^{WT} to FITC-cRGD (5 nM) can be inhibited by Ca^{2+}, no effect was shown in the ADMIDAS mutant. Titrations were done in triplicate.

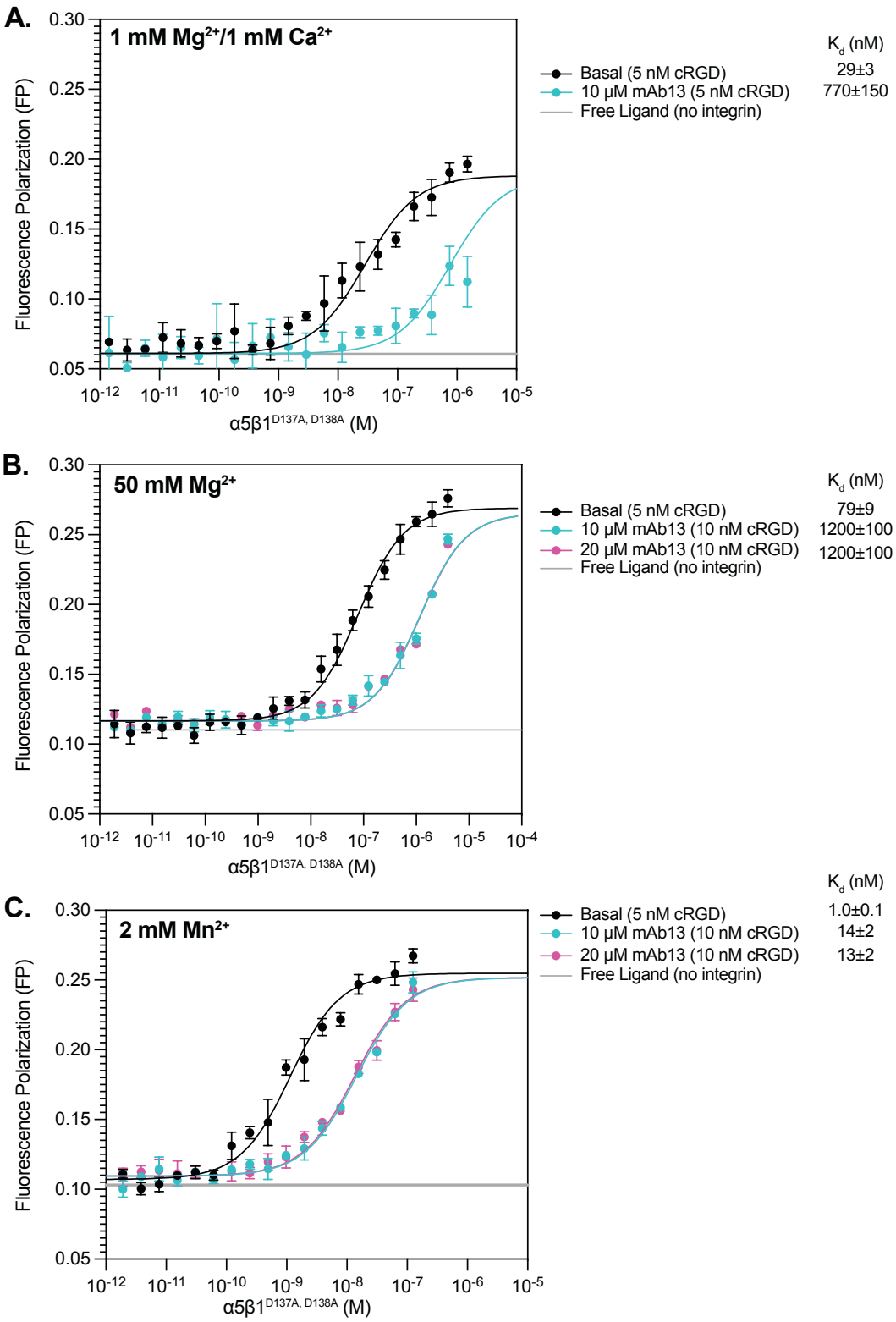

Figure S5. Basal and closed ensemble affinities of α5β1$^{D137A, D138A}$ for FITC-cRGD. (A-C) The basal and closed ensemble affinity were determined in 1 mM Mg^{2+} / 1 mM Ca^{2+} (A), 50 mM Mg^{2+} (B), and 2 mM Mn^{2+} (C), by titrating α5β1$^{D137A, D138A}$ in the absence and presence of Fab mAb13. In the experiments containing 50 mM Mg^{2+} and 2 mM Mn^{2+}, titrations were done in two concentrations of mAb13 to ensure full satuation of the closed ensemble. Titrations were done in triplicate and fitted affinities can be found in Table 1. Basal affinities were measured three (A) and five times (B) and averaged.

Table S1. EC_{50}s of Fab titrations α5β1^{WT} and α5β1$^{D137A, D138A}$ in different metal ion conditions.
Graphs of the titrations can be found in Figure 3. Concentrations of integrin and ligand can be found in Table S2.

		α5β1^{WT}			α5β1$^{D137A, D138A}$		
		1 mM Mg^{2+} 1 mM Ca^{2+}	**50 mM Mg^{2+}**	**2 mM Mn^{2+}**	**1 mM Mg^{2+} 1 mM Ca^{2+}**	**50 mM Mg^{2+}**	**2 mM Mn^{2+}**
●●	**HUTS4** (nM)	20±3	8.5±2.0	-	120±170	120±120	14±6
□	**12G10** (nM)	1.1±0.2	0.74±0.16	-	0.065±0.015	0.80±0.22	0.22±0.05
▲	**9EG7** (nM)	3.1±1.4	-	-	-	-	-
▽	**8E3** (nM)	8.9±3.8	6.3±3.3	-	1.6±1.4	-	-
◆	**SG/19** (nM)	5.1±1.7	1.5±0.3	-	14±6	10±3	3100±450
○	**mAb13** (nM)	2.3±1.1	3.5±0.4	-	23±2	18±3	0.98±0.27

Table S2. Concentrations of α5β1 and ligand used in Fab titrations of α5β1^{WT} and α5β1$^{D137A, D138A}$ (Figure 3, Table S1).

	α5β1^{WT}						α5β1$^{D137A, D138A}$					
	1 mM Mg^{2+} 1 mM Ca^{2+}		50 mM Mg^{2+}		2 mM Mn^{2+}		1 mM Mg^{2+} 1 mM Ca^{2+}		50 mM Mg^{2+}		2 mM Mn^{2+}	
	α5β1^{WT}	RGD	α5β1^{WT}	RGD	α5β1^{WT}	RGD	α5β1^{mut}	cRGD	α5β1^{mut}	cRGD	α5β1^{mut}	cRGD
HUTS4 (nM)	20	5	50	5	5	5	10	10	10	10	10	10
12G10 (nM)	20	5	50	5	5	5	10	10	10	10	10	10
9EG7 (nM)	20	5	50	5	5	5	50	10	50	10	10	10
8E3 (nM)	20	5	50	5	5	5	50	10	50	10	10	10
SG/19 (nM)	20	5	50	5	20	5	100	10	100	10	10	10
mAb13 (nM)	20	5	50	5	20	5	100	10	100	10	10	10

Table S3. Fitted K_d values for $\alpha5\beta1^{WT}$ and $\alpha5\beta1^{D137A, D138A}$ in the presence and absence of saturating concentrations of Fabs. Graphs of the titrations can be found in Figure 4, fitted values from panel A can be found in Li et al. {Li, 2017 #24745}.

		$\alpha5\beta1^{WT}$		$\alpha5\beta1^{D137A, D138A}$		
		50 mM Mg^{2+}	**2 mM Mn^{2+}**	**1 mM Mg^{2+} 1 mM Ca^{2+}**	**50 mM Mg^{2+}**	**2 mM Mn^{2+}**
●	**Basal** (nM)	62±4	2.8±0.3	24000±3600	14000±1300	580±62
○	**HUTS4** (nM)	26±2	1.5±0.2	630±54	730±53	51±6
□	**12G10** (nM)	-	1.7±0.3	170±14	1000±76	14±2
▲	**9EG7** (nM)	53±3	3.3±0.4	-	-	-
▼	**8E3** (nM)	54±3	2.2±0.3	-	-	-
●	**mAb13,** 15 µM (nM)	48000±8500	3200±130	-	-	-
●	**mAb13,** 30 µM (nM)	51000±9500	3500±140	-	-	-